Travail de fin d'études en chimie et bio-industries : Chemical Pretreatment-Assisted Refining of Textile Waste Fibres for Construction Applications.

Auteur : Afridi, Muhammad Faisal
Promoteur(s) : Richel, Aurore; 31392; 31393
Faculté : Gembloux Agro-Bio Tech (GxABT)
Diplôme : Master en bioingénieur : chimie et bioindustries, à finalité spécialisée
Année académique : 2025-2026
URI/URL : http://hdl.handle.net/2268.2/26057

European Master in Biological and Chemical Engineering for a Sustainable Bioeconomy

BIOCEB MASTER PROGRAMME

Master Thesis Report

Submitted to obtain the degrees of:

- Master in biology AgroSciences (BAS) – University of Reims Champagne-Ardenne
- Master of Science in Engineering – Tallinn University of Technology
- Master in Bioengineering: Chemistry and Bioindustries – University of Liège

Chemical Pretreatment–Assisted Refining of Textile Waste Fibres for Construction Applications

Author: Muhammad Faisal AFRIDI

Defence date: 22 / 06 / 2026

Thesis Supervisor: Prof. Bruno Dufau Mattos
Thesis Advisors: Meri Lundahl (PhD), Saija Rantanen (PhD)
at Aalto University, School of Chemical Engineering, Department of Bioproducts and Biosystems, P.O. Box 16300, FI-00076 AALTO, Finland
from 05/01/2026 to 31/05/2026

Bioceb Supervisors:
Prof. RICHEL, Aurore (Université de Liège)
Prof. PLAMUS, Tiia (Tallinn University of Technology)

Confidentiality: No

Statement of responsibility

This document is the sole responsibility of its author

Table of Contents

List of Figures

List of Tables

List of Appendices

PREFACE

This master's thesis was carried out at Aalto University, School of Chemical Engineering, Department of Bioproducts and Biosystems, within the BIOCEB programme. The work focuses on the chemical pretreatment and mechanical refining of recycled textile fibres and their potential use in lightweight construction materials.

I would like to sincerely thank my supervisor, Prof. Bruno Dufau Mattos, for his guidance, support, and valuable feedback throughout this research. I am also deeply grateful to my advisor, Meri Lundahl, for her continuous encouragement, insightful discussions, and support at every stage of this thesis project. I would also like to thank Saija Rantanen for her valuable guidance and assistance during the course of this thesis project.

Special thanks to Roozbeh Abidnejad and Rosangela A. Maia for their guidance, and to my colleagues Pedro Martinez and Fahad Muhammad Imran for their support and discussions throughout the work. Their input played an important role in shaping this study.

I am also grateful to everyone in the group who contributed to this work through discussions, technical assistance, and day-to-day laboratory support. Their assistance played an important role in the progress of this project and made the working environment very supportive and enjoyable.

Lastly, I would like to thank my family and friends for their constant encouragement, patience, and support throughout my studies. Their belief in me has meant more than words can express.

Espoo, 15 June 2026

Muhammad Faisal Afridi

List of abbreviations and symbols

Cot-AcA	Cotton fibres treated with acetic acid
Cot-Ctrl	Cotton fibres water-soaked control
Cot-NaU	Cotton fibres treated with NaOH/urea
PC-AcA	Polycotton fibres treated with acetic acid
PC-Ctrl	Polycotton fibres water-soaked control
PC-NaU	Polycotton fibres treated with NaOH/urea
PET-AcA	PET fibres treated with acetic acid
PET-Ctrl	PET fibres water-soaked control
PET-NaU	PET fibres treated with NaOH/urea
ATR-FTIR	Attenuated Total Reflectance Fourier-Transform Infrared Spectroscopy
	Au/Pd Gold/Palladium (sputter coating alloy)
CI	Crystallinity Index
DMC	Dry Matter Content
FWHM	Full Width at Half Maximum
GC-MS	Gas Chromatography-Mass Spectrometry
HPLC	High-Performance Liquid Chromatography
LVR	Linear Viscoelastic Region
MFC	Microfibrillated Cellulose
NaOH	Sodium Hydroxide (caustic soda)
O/C	Oxygen-to-Carbon atomic ratio (XPS surface indicator)
PET	Polyethylene Terephthalate
pH	Potential of Hydrogen (acidity/basicity scale)
QBSD	Quadrant Backscattered Electron Detector
SDS	Sodium Dodecyl Sulphate
SEM	Scanning Electron Microscopy
TPU	Thermoplastic Polyurethane
WRV	Water Retention Value
wt%	Weight percent
XPS	X-ray Photoelectron Spectroscopy
XRD	X-ray Diffraction

Abstract

This study investigated the effects of alkaline NaOH/urea (5/12 wt%) and concentrated acetic acid (50 wt%) pretreatments on recycled cotton, polyethylene terephthalate (PET), and 50/50 polycotton fibres. The fibres were studied both before and after mechanical refining to evaluate their suitability for lightweight fibre-based construction foams. Fibres were characterised by water retention value (WRV), ATR-FTIR spectroscopy, scanning electron microscopy (SEM), X-ray diffraction (XRD), and X-ray photoelectron spectroscopy (XPS). In addition polycotton suspensions were further evaluated by oscillatory rheometry, Turbiscan optical stability analysis, and gravimetric foam characterisation.

NaOH/urea pretreatment increased the WRV of cotton by 12.1% and, after refining, led to extensive longitudinal fibril delamination. The surface O/C ratio also increased from 0.57 to 0.62, together with near-complete removal of nitrogen-containing sizing agents, indicating improved surface purification and greater cellulose exposure. A weak carbonyl band at 1710 cm^{-1} was observed in all cotton samples, but it was noticeably stronger in the NaOH/urea-treated sample (Cot-NaU), which may be linked to mild alkaline oxidation or partial carbamate formation.

In contrast, acetic acid pretreatment reduced the WRV of cotton by 9.4%, suggesting inter-fibrillar consolidation and selective hydrolysis of amorphous cellulose. This was supported by a slight increase in crystallinity index (70.26% compared to 68.65% for Cot-Ctrl). PET fibres remained chemically unaffected under both pretreatment conditions.

In polycotton, the effects of both pretreatments were noticeably weaker compared to pure cotton across all characterisation methods. This is likely due to physical and capillary constraints introduced by the PET component. PC-NaU formed a much stronger viscoelastic gel (G'_0 = 2,970 Pa) than PC-AcA (G'_0 = 454 Pa). It also showed better sedimentation stability over 60 minutes and produced foams with a denser fibrillar structure and lower bulk porosity (60.07% compared to 67.56% for PC-Ctrl).

These results demonstrate that the type of chemical pretreatment strongly influences fibrillation behaviour and network-forming capacity of recycled textile

fibres. Among the two pretreatments, NaOH/urea proved to be more effective in generating stable, processable fibre suspensions for construction applications.

Keywords: Textile waste recycling, cotton, polyethylene terephthalate, polycotton, alkaline pretreatment, acid pretreatment, mechanical refining, fibre modification, foam, circular economy

Résumé

Cette étude a examiné les effets des prétraitements alcalins NaOH/urée (5/12 % en poids) et à l'acide acétique concentré (50 % en poids) sur des fibres de coton recyclé, de polyéthylène téréphtalate (PET) et de polycoton 50/50. Les fibres ont été étudiées avant et après raffinage mécanique afin d'évaluer leur aptitude à la production de mousses légères à base de fibres pour la construction. Les fibres ont été caractérisées par leur valeur de rétention d'eau (WRV), spectroscopie ATR-FTIR, microscopie électronique à balayage (SEM), diffraction des rayons X (XRD) et spectroscopie de photoélectrons X (XPS). De plus, les suspensions de polycoton ont été évaluées par rhéométrie oscillatoire, analyse de stabilité optique Turbiscan et caractérisation gravimétrique des mousses.

Le prétraitement NaOH/urée a augmenté la WRV du coton de 12,1 % et, après raffinage, a conduit à une importante délamination longitudinale des fibrilles. Le rapport O/C en surface est également passé de 0,57 à 0,62, ainsi qu'une élimination quasi complète des agents d'encollage azotés, indiquant une meilleure purification de surface et une plus grande exposition de la cellulose. Une faible bande carbonyle à 1710 cm^{-1} a été observée dans tous les échantillons de coton, mais elle était nettement plus marquée dans l'échantillon traité par NaOH/urée (Cot-NaU), ce qui pourrait être lié à une oxydation alcaline modérée ou à une formation partielle de carbamate.

En revanche, le prétraitement à l'acide acétique a réduit la WRV du coton de 9,4 %, suggérant une consolidation interfibrillaire et une hydrolyse sélective de la cellulose amorphe. Ceci a été soutenu par une légère augmentation de l'indice de cristallinité (70,26 % contre 68,65 % pour Cot-Ctrl). Les fibres de PET sont restées chimiquement inchangées dans les deux conditions de prétraitement.

Dans le polycoton, les effets des deux prétraitements étaient nettement plus faibles par rapport au coton pur pour toutes les méthodes de caractérisation. Cela est probablement dû aux contraintes physiques et capillaires induites par le composant PET. Le PC-NaU a formé un gel viscoélastique beaucoup plus rigide (G'_0 = 2 970 Pa) que le PC-AcA (G'_0 = 454 Pa). Il a également montré une meilleure stabilité à la sédimentation sur 60 minutes et a produit des mousses

avec une structure fibrillaire plus dense et une porosité apparente plus faible (60,07 % contre 67,56 % pour PC-Ctrl).

Ces résultats démontrent que le type de prétraitement chimique influence fortement le comportement à la fibrillation et la capacité de formation de réseau des fibres textiles recyclées. Parmi les deux prétraitements, le NaOH/urée s'est avéré plus efficace pour générer des suspensions de fibres stables et aptes à la transformation pour des applications dans le secteur de la construction.

Mots-clés : Recyclage des déchets textiles, coton, polyéthylène téréphtalate, polycoton, prétraitement alcalin, prétraitement acide, raffinage mécanique, modification des fibres, mousse, économie circulaire

1. Introduction

The rapid growth of the global textile industry has led to a significant increase in textile waste generation, posing serious environmental and economic challenges. Recent studies indicate that over 92 million tonnes of textile waste are generated worldwide each year, and this number is expected to increase due to the rising consumption and fast fashion trends [1]. China and the United States produce the largest shares, at 20 million tonnes and 17 million tonnes, respectively [2]. Within the European Union, around 16 million tonnes of textile wastes are produced annually, of which only about 26% is recycled [3]. The majority of this recycled material is downcycled into low-value applications such as insulation materials and fillers. As a result, less than 1% is returned to new textile fibres, highlighting the limited progress toward a circular textile economy [4].

The growing textile production and waste accumulation have significant environmental implications. The textile industry accounts for around 10% of global greenhouse gas emissions making it a major contributor to climate change [5]. It is also a significant source of plastic pollution. It generates approximately 42 million tonnes of plastic waste annually, second only to the packaging sector[6]. In addition, the industry is also the second-largest contributor to global carbon and water footprints, after oil and gas exploration [7]. These impacts are largely driven by fast fashion trends, short textile product lifespans, and limited recycling infrastructure.

In response to these challenges, there is also increasing interest in the transitioning from a linear to a circular economy model for textile recycling [8]. Within the framework of the circular economy, textile waste is no longer consider as a disposal problem but as a potential secondary resource. [9]. Different Valorisation strategies used aim to recover value from waste materials and reintroduce them into the production cycle.

Various recycling strategies have been explored, including mechanical, chemical and biological approaches. Mechanical recycling of post-consumer textile waste remains limited due to the complexity of mixed-fibre compositions, which are difficult to process efficiently. In addition, shredding processes reduce fibre length and quality. The resulting fibres are typically shorter and weaker, which often necessitates the use of virgin materials to achieve the desired performance [10]

[11]. In contrast, chemical recycling enables the recovery of polymers and fibres through processes such as depolymerisation, dissolution, and regeneration. This makes it particularly relevant for complex textile streams such as cotton–polyester blends [12]. However, these approaches are primarily focused on material recovery at the polymer level and mostly it involves high energy input and multiple processing steps, which ultimately can limit their scalability and sustainability. This creates a need for the alternative strategies that enable the direct utilization of the textile waste fibres in value-added applications.

One promising pathway is the use of textile waste fibres in fibre-based construction materials, particularly in porous and lightweight structures such as insulation panels, acoustic materials, and foam-like architectures. In these applications, the formation of stable, interconnected fibre networks is essential to achieve low density, high porosity, and sufficient mechanical integrity. However, a key limitation is the refining behaviour of textile fibres. Unlike lignocellulosic fibres, textile fibres such as cotton and polyethylene terephthalate (PET) exhibit limited swelling and significant rigidity. This restricts fibrillation and instead promotes fibre cutting during mechanical processing. [13]. This results in shorter fibres with reduced capacity for inter-fibre bonding, ultimately hindering the formation of cohesive networks which is required for foam-like structures.

To address these challenges, chemical pretreatment can be employed to modify fibre structure prior to mechanical refining. Such chemical treatments can enhance swelling, alter surface chemistry, and partially disrupt the crystalline regions, thereby promoting fibrillation over cutting [14]. This transition is essential for improving fibre flexibility, increasing surface area, and facilitating the formation of interconnected fibre networks suitable for porous and foam-based materials. Accordingly, this study hypothesizes that chemical pretreatment enables more effective refining of textile waste fibres for construction foam applications. Unlike prior work focused on pure cellulose, this study extends the approach to polycotton blends. It directly links pretreatment-induced structural changes to suspension rheology and foam formation.

2. State of the Art

This chapter reviews the current state of the art in the processing and utilization of textile waste fibres, with a focus on their potential application in lightweight and porous construction materials. It focuses on the structural features of common textile fibres, how they behave during processing, and the key limitations of conventional recycling methods. It also discusses mechanical and chemical approaches used to modify fibre properties. Special attention is given on their combined role in improving refining efficiency. Finally, the formation of fibre networks in foam-based systems is considered, which highlights the key factors required to enable the use of textile waste in such kind of applications.

2.1 Textile Waste as a Fibre Resource

Textile waste consists of a wide variety of natural and synthetic fibres, with cotton and polyethylene terephthalate (PET) being the most common [14]. These fibres differ strongly in their chemical structure, morphology, and physicochemical properties, which in turn govern their behavior during recycling and processing. Understanding these differences is essential for developing effective strategies for fibre modification, refining, and subsequent material applications. This becomes especially important in mixed textile streams, where cotton and PET respond very differently to mechanical and chemical treatments [[15] [16]. For this reason, cotton, PET, and their blends are discussed separately in this section to highlight their individual characteristics and recycling implications.

2.1.1 Cotton

Cotton is a natural cellulosic fibre composed primarily of cellulose, a linear polysaccharide consisting of β-(1→4)-linked D-glucose units [17]. Structurally, It contains both crystalline and amorphous regions, along with a high density of hydroxyl groups, which contribute to its hydrophilic nature and ability to swell in aqueous environments [18] [19]. The molecular structure of cellulose is illustrated in Figure 1, showing the presence of hydroxyl groups responsible for hydrogen bonding and swelling behaviour. This swelling behaviour increases fibre flexibility and facilitates mechanical processing, particularly fibrillation during refining [20].

However, post-consumer cotton derived from garments is often subject to extensive hornification before recycling. This occurs because repeated washing and drying cycles during the service life of clothing gradually reduce the fibre's ability to re-swell. More significantly, mechanical shredding and carding during recycling lead to a substantial reduction in staple length. This reduces yarn strength, spinning efficiency, and the capacity for inter-fibre bonding during subsequent processing [21], [22]. As a result, although cotton is inherently more processable than synthetic fibres due to its hydrophilic nature, its performance in recycled form is mainly limited by reduced fibre length rather than changes in its chemical structure.

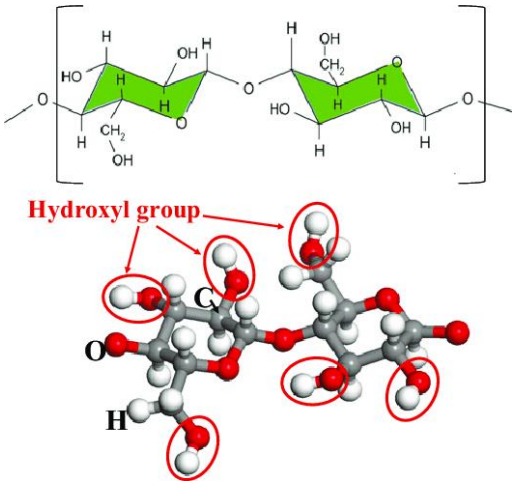

Figure 1: Chemical structure of cellulose showing linked glucose units and hydroxyl functional groups responsible for hydrogen bonding and swelling behaviour. (Adapted from [23])

2.1.2 Polyethylene terephthalate (PET)

Polyethylene terephthalate (PET) is a synthetic thermoplastic polyester with a semi-crystalline structure, consisting of both amorphous and crystalline regions. Its physical appearance, ranging from transparent to opaque, depends on the relative proportion and distribution of these phases [24]. is extensively utilized in both rigid and flexible packaging, textile manufacturing, thermoformed products, and as a component in glass fibre–reinforced engineering resins [25]. It consists of repeating ester-linked units derived from terephthalic acid and ethylene glycol [26] as shown in figure 2. Unlike cellulose, PET lacks hydrophilic functional groups, resulting in a predominantly hydrophobic character [27] and negligible swelling in aqueous systems.

This structural rigidity and resistance to chemical penetration make PET fibres difficult to process using conventional mechanical refining techniques [28]. Instead of undergoing fibrillation, PET fibres tend to resist deformation or fracture into shorter segments under mechanical stress [29]. Consequently, their contribution to fibre network formation is limited, particularly in applications requiring strong inter-fibre bonding.

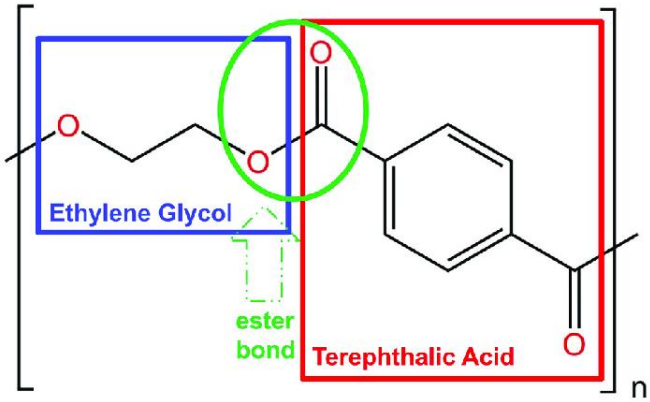

Figure 2: Chemical structure of PET, illustrating ester linkages and aromatic rings responsible for its rigidity and hydrophobic nature. (Adapted from [30])

2.1.3 Cotton–PET Blends

In blended textile systems, cotton and PET fibres coexist within a single material, combining hydrophilic and hydrophobic components with fundamentally different structural characteristics. This heterogeneity creates significant challenges during recycling and processing. The two fibre types respond differently to both mechanical and chemical treatments [31].

2.2 Processing Strategies for Textile Waste Fibres

The conversion of textile waste into functional materials requires a combination of processing strategies that modify fibre morphology and interfacial properties. These strategies can generally be grouped into mechanical, chemical, and biological approaches, each targeting different limitations of textile fibres [29]. Mechanical processes mainly affect fibre size and structure, while chemical treatments are used to alter internal organization and surface properties. Biological methods, typically based on enzymes or microorganisms, provide a more environmentally friendly alternative by selectively modifying fibre

components under mild conditions. However, their use in textile fibre refining is still limited due to slower processing compared to conventional approaches [32].

2.2.1 Mechanical Processing and Refining

Mechanical recycling of textiles refers to the recovery of fibres through physical processes without the use of chemical treatments. It typically includes operations such as shredding, cutting, tearing, grinding, or garneting to break down textile waste into reusable fibrous material [33]. Through these processes, textile waste can be converted into reusable products without significantly changing the chemical composition of the material [34]. Natural fibre waste is often processed by shredding, followed by techniques such as heat pressing or needle punching to produce nonwoven materials. These are commonly used in applications such as agricultural geotextiles, composite reinforcement, and thermal and acoustic insulation. In comparison, synthetic fibres such as polyester or nylon are typically subjected to melting and fragmentation into flakes or pellets. These fibres are then re-extruded and spun into new fibres [35].

Although mechanical recycling has been used for decades, the recovered fibres are often of lower value due to harsh tearing and shredding operations that reduce fibre length [36]. In addition, this method is most effective for single-fibre fabrics and can cause greater damage to natural fibres than to synthetics in blended textiles. As a result, it is less suitable for mixed-material fabrics like cotton and PET blend [37].

2.2.2 Chemical Pretreatment Approaches

Chemical recycling of textile waste involves the use of solvents, reagents, or other chemical agents to modify the chemical structure and properties of fibres. Unlike mechanical methods, chemical treatments can penetrate the internal structure of fibre, promoting depolymerisation and surface modification, which enhances fibre flexibility and facilitates subsequent processing. [38]. Chemical recycling is often challenged by the diversity of fabrics, the presence of dyes, and various functional textile finishes. These residual substances on textile waste can interfere with the recycling process, which leads to complications and reduced efficiency [39].

2.2.2.1 Alkali Pretreatment

Alkali pretreatment involves treating textile waste with bases such as sodium, potassium, calcium, or ammonium hydroxides to modify structure of fibre and enhance their processability [40]. The primary role of alkaline treatment on cellulose is to induce swelling. This disrupts the inter- and intra-molecular hydrogen bonds within the cellulose structure, thereby increasing the proportion of amorphous regions [41]. Sodium hydroxide hydrates penetrate the amorphous regions of cellulose and disrupt the crystalline domains, enhancing the dissolution of cotton cellulose [42]. Concurrently, urea hydrates inhibit the re-association of cellulose molecules by acting as both hydrogen bond donors and acceptors, which further promote fibre separation and flexibility during refining [43]. Alkaline hydrolysis using NaOH, often with a phase transfer catalyst, effectively depolymerizes PET at moderate temperatures and 5–15% NaOH. Hydroxide ions cleave the ester bonds in PET, producing disodium terephthalate and ethylene glycol, which are both soluble in water [42] [43].

2.2.2.2 Acidic Pretreatment

Acidic pretreatment of textile fibres involves the use of mild acids, such as acetic, sulfuric acids or phosphoric acids, to modify fibre structure and surface properties, thereby enhancing their processability [46] [47]. For cellulosic fibres such as cotton, acid treatment can disrupt inter- and intra-molecular hydrogen bonding and partially depolymerise amorphous cellulose regions, which may promote flexibility and fibre separation. However, the effect on water uptake by the fibre is concentration-dependent and not straightforward. While dilute acid treatment may increase accessibility by opening inter-fibrillar spaces, concentrated acid exposure can instead promote direct cellulose–cellulose bond formation upon acid removal. This can lead to inter-fibrillar consolidation and irreversible pore closure, thereby reducing water retention capacity [48], [49]. This dual behaviour should therefore be considered when interpreting the downstream effects of acidic pretreatment on cotton swelling and processability. For synthetic polyester s, acids can in principle cleave the ester bonds in the PET backbone through proton-assisted hydrolysis, generating terephthalic acid and ethylene glycol as degradation products [50]. Under the mild ambient conditions typically used in pretreatment, significant bulk depolymerisation of PET is unlikely. However, surface-level ester hydrolysis may

still occur. This can lead to changes in surface chemistry and improved interfacial compatibility in blended systems.

3. Material and Methods

This chapter describes the materials, experimental procedures, and characterisation methods used in this study. The experimental workflow was carried out in four sequential stages: (i) surface cleaning of raw textile fibres using dilute sulphuric acid washing; (ii) chemical pretreatment using either alkaline (NaOH/urea) or acidic (acetic acid) media; (iii) mechanical refining via high-shear processing; and (iv) physicochemical characterisation of the resulting fibre suspensions.

An overview of the experimental workflow is shown in Figure 3.

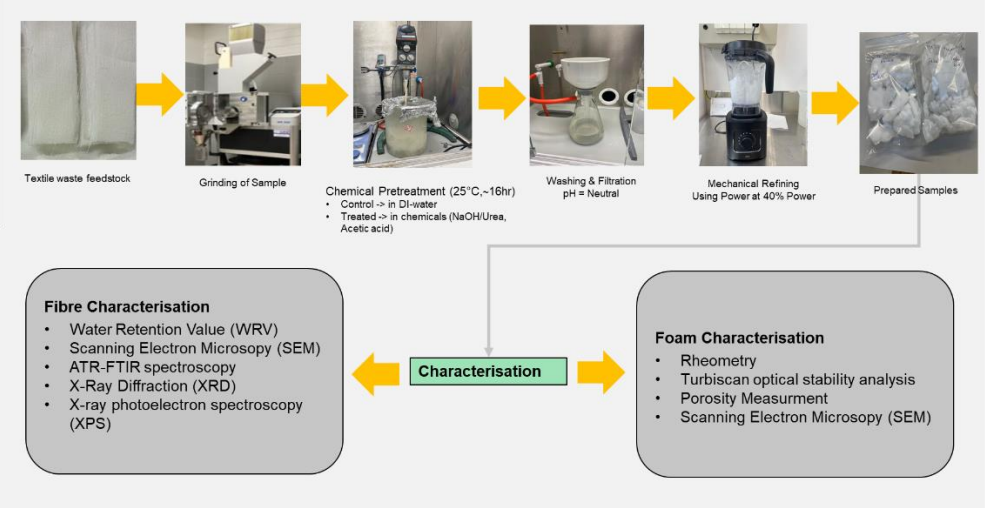

Figure 3: Schematic representation of the experimental workflow

3.1 Raw Materials

3.1.1 Textile Fibres

Three textile fibre types were selected as model substrates representing the compositional range of post-consumer textile waste: 100% cotton, 100% polyethylene terephthalate (PET), and a 50/50 (w/w) cotton–PET blend (polycotton). Cotton fibres were supplied by Rester (Finland) as mechanically recycled post-consumer textile waste with an average fibre length of approximately 1.5 mm. PET and polycotton fabrics were purchased from Eurokangas (Finland) and used as artificial waste, as no local supplier was found for mechanically recycled short s of PET or polycotton. All materials were white and used as received prior to surface cleaning.

3.1.2 Chemicals and Reagents

All chemicals were used as received without further purification. Sodium hydroxide (NaOH, ≥97%, analytical grade, Sigma-Aldrich), urea (CH_4N_2O, ≥99%, analytical grade, Sigma-Aldrich), glacial acetic acid (CH_3COOH, 100%, Emparta ACS, Merck KGaA), concentrated sulphuric acid (H_2SO_4, 98%, analytical grade, Sigma-Aldrich), sodium dodecyl sulphate (SDS, ≥99%, analytical grade, Sigma-Aldrich), and methylcellulose (Sigma-Aldrich) were used throughout this study. All solutions were prepared using deionised water unless stated otherwise.

3.2 Surface Cleaning by Dilute Sulphuric Acid Washing

Prior to chemical pretreatment, all three fibre types were subjected to a dilute sulphuric acid washing step to remove surface finishing agents, sizing compounds, and softeners that could otherwise impede reagent access to the fibre surface. Cotton fibres as well as PET and Polycotton Fabrics were immersed in a 0.01 M H_2SO_4 solution at 40 °C for 40 minutes with manual stirring at 10-minute intervals. Following immersion, excess liquid was removed by mechanical spinning and the textiles were rinsed in a laboratory washing machine (Electrolux FOM71) to neutralise and remove residual acid. The cleaned textiles were dried at 40 °C.

After drying, the PET and Polycotton fabrics were cut into approximately 5 × 10 cm pieces using electric scissors to facilitate subsequent size reduction and uniform feeding into the cutting mill. The pre-cut samples were then processed using a Retsch SM 300 Cutting Mill equipped with a 4 mm sieve. Milling produced uniformly sized fibrous material suitable for subsequent chemical pretreatment and suspension preparation.

3.3 Chemical Pretreatment

Chemical pretreatment was applied to modify fibre structure prior to mechanical refining, with the objective of promoting fibrillation. Two reagent systems were evaluated — an alkaline NaOH/urea solution and a concentrated acetic acid solution — together with a water-soaked control as shown in table 1. All three fibre types (cotton, PET, and polycotton) were subjected to each treatment condition, yielding nine fibre groups in total.

Pretreatment solutions were prepared at the following concentrations: NaOH and urea at 5 wt% and 12 wt%, respectively, in deionised water; and acetic

acid at 50 wt% in deionised water. For the control, fibres were immersed in deionised water under identical conditions. In each case, the milled fibre material was immersed in the pretreatment solution at a dry fibre loading of 20 g/L and mixed thoroughly using an overhead stirrer. Immersion was carried out overnight (approximately 16 hours) at ambient temperature, with the mixing speed of 200 rpm.

After treatment, the fibres were recovered by vacuum filtration and washed thoroughly with deionised water. This was done by re-suspending the filter cake in ~3 L of water, stirring for 30 minutes at 350 rpm, and re-filtering. The washing step was repeated at least three times and continued until neutral pH was reached. Finally, the dry matter content (DMC) of each sample was measured in duplicate using a moisture analyser, with approximately 0.5 g of wet sample placed on an aluminium plate for each measurement.

Table 1: Summary of chemical pretreatment conditions applied to all three fibre types.

Sample Code	Fibre type	Treatment	Reagent concentration	Fibre loading	Immersion time
Cot-Ctrl	Cotton	Control	Deionised water	20 g/L	Overnight (~16 h)
Cot-NaU	Cotton	NaOH/urea	5 wt% NaOH / 12 wt% urea	20 g/L	Overnight (~16 h)
Cot-AcA	Cotton	Acetic acid	50 wt% CH_3COOH	20 g/L	Overnight (~16 h)
PET-Ctrl	PET	Control	Deionised water	20 g/L	Overnight (~16 h)
PET-NaU	PET	NaOH/urea	5 wt% NaOH / 12 wt% urea	20 g/L	Overnight (~16 h)
PET-AcA	PET	Acetic acid	50 wt% CH_3COOH	20 g/L	Overnight (~16 h)
PC-Ctrl	Polycotton	Control	Deionised water	20 g/L	Overnight (~16 h)
PC-NaU	Polycotton	NaOH/urea	5 wt% NaOH / 12 wt% urea	20 g/L	Overnight (~16 h)
PC-AcA	Polycotton	Acetic acid	50 wt% CH_3COOH	20 g/L	Overnight (~16 h)

3.4 Mechanical Refining by Blending

After chemical pretreatment and washing, all fibre suspensions were diluted with deionised water to a consistency of 2 wt% (dry fibre basis), with a maximum batch volume of 2 L. Mechanical refining was then carried out using a Witt Premium Power Blender (WPB1500B, 1500 W) operated at 40% speed for 3 minutes. The same conditions were applied to all nine fibre groups to ensure comparable mechanical energy input.

After refining, the suspensions were recovered by vacuum filtration. The filtrate was collected and poured back over the filter cake to minimise loss of fine fibre fragments. The wet fibre cakes were then transferred into sealed ziplock bags, manually homogenised by squeezing, and left overnight to equilibrate moisture content.

Finally, DMC was measured in duplicate using a moisture analyser.

3.5 Physicochemical Characterisation

The processed fibre suspensions were analysed using four complementary techniques: water retention value (WRV), attenuated total reflectance Fourier-transform infrared spectroscopy (ATR-FTIR), scanning electron microscopy (SEM), and X-ray diffraction (XRD). Each method provides information on a different aspect of fibre structure, and together they allow a more complete understanding of how chemical pretreatment and mechanical refining influence fibre morphology, surface chemistry, and crystalline structure. For ATR-FTIR and XRD measurements, fibre samples were dried in a forced-convection oven at 65 °C for 24 hours prior to analysis to eliminate adsorbed moisture that would otherwise interfere with spectral and diffraction data.

3.5.1 Water Retention Value

WRV was determined according to SCAN-C 102:XE with minor procedural adaptations. The measurement quantifies water retained within the inter-fibrillar pore structure after centrifugation, expressed as grams of water per gram of dry fibre (%).

Prior to centrifugation, the DMC of each sample was adjusted to approximately 15 wt% using deionised water. Aliquots of 10.27 g (wet basis) were placed on wire mesh sample cups fitted with aluminium sleeves and centrifuged at 3000 × g for 15 minutes (Thermo Fisher Scientific SL40FR). The centrifuged wet samples were immediately weighed, dried overnight at 105 °C, cooled in a desiccator, and re-weighed. WRV was calculated as:

$$WRV(\%) = \frac{m_{wet} - m_{dry}}{m_{dry}} \times 100 \quad (1)$$

where *m_wet* and *m_dry* are the masses of the centrifuged wet and oven-dried samples, respectively. All measurements were performed in triplicate.

3.5.2 ATR-FTIR Spectroscopy

Infrared spectroscopic characterisation was performed using a PerkinElmer FTIR spectrometer equipped with a single-bounce attenuated total reflectance (ATR) accessory. Dried fibre samples were placed directly on the ATR crystal and sufficient contact pressure was applied to ensure reproducible optical contact between sample and crystal. Spectra were collected over the wavenumber range 4000–500 cm^{-1} at a spectral resolution of 4 cm^{-1}, with 16 co-added scans per spectrum. A background spectrum was acquired under identical conditions prior to each sample measurement.

3.5.3 Scanning Electron Microscopy

Prior to imaging, all fibre samples were freeze-dried for 72 hours and sputter-coated with a gold/palladium (Au/Pd) alloy using a Quorum Q150R sputter coater to ensure electrical conductivity. SEM imaging was performed using a Phenom Pure G5 desktop SEM (Thermo Fisher Scientific, Netherlands) equipped with a quadrant backscattered electron detector (QBSD) at an accelerating voltage of 5.3 kV and a working distance in the range of 6–7 mm. Representative micrographs were collected for all fibre types — cotton, PET, and polycotton — under each treatment condition (control, NaOH/urea, and acetic acid) in both unrefined and refined states. For cotton and PET fibres, images were acquired at 1000× magnification to capture overall morphology and surface texture. For NaOH/urea- and acetic acid-treated polycotton samples, additional images were taken at

2000× to resolve finer fibrillar features. Foam preparation and SEM imaging conditions are described in the Foam Preparation and Characterisation subsection.

3.5.4 X-ray Diffraction

Wide-angle X-ray diffraction (XRD) measurements were performed on a Malvern Panalytical Aeris diffractometer equipped with a Cu Kα X-ray source (λ = 1.5406 Å), a PIXcel1D detector, and a sample spinner. The instrument was operated at 40 kV and 7.5 mA. Diffractograms were collected over the 2θ range of 10–50° with a step size of 0.0217°.

The crystallinity index (CI) was determined by Gaussian peak deconvolution rather than the Segal empirical method, as the latter has been shown to overestimate crystallinity by including contributions from oriented amorphous cellulose in the crystalline peak intensity [51] [52]. For cotton samples, a four-peak deconvolution model was applied comprising the ($1\bar{1}0$), (110), (002), and (040) crystalline reflections of cellulose I together with a single broad amorphous Gaussian component. For PET samples, a three-peak model was used comprising the ($1\bar{1}0$)/(010), (110), and (100) reflections of the triclinic PET unit cell together with one amorphous Gaussian. The CI was calculated as:

$$\mathrm{CI}(\%) = \frac{\sum \mathrm{A_{cryst}}}{\sum \mathrm{A_{cryst}} + \mathrm{A_{am}}} \times 100 \qquad (2)$$

where ΣA_cryst is the sum of the areas of all crystalline Gaussian peaks and A_am is the area of the amorphous Gaussian component. All deconvolution fits achieved $R^2 \geq 0.995$.

The apparent crystallite size (L) along the primary reflection direction was estimated using the Scherrer equation [51].

$$\mathrm{L} = \frac{\mathrm{K}\lambda}{\beta \cos\theta} \qquad (3)$$

where K = 0.9 is the dimensionless shape factor, λ = 1.5406 Å is the Cu Kα wavelength, β is the full width at half maximum (FWHM) of the fitted Gaussian peak in radians, and θ is the Bragg angle of the corresponding reflection.

The interplanar d-spacing was calculated from the peak position using Bragg's law:

$$n\lambda = 2d_{hkl}\sin\theta \qquad (4)$$

where *n* is the diffraction order, λ = 1.5406 Å is the Cu Kα wavelength, and θ is the Bragg angle. Only the first-order reflection (n = 1) was considered, since higher-order reflections were either outside the measured 2θ range or too weak to detect. This gives d□□□ = λ / (2 sinθ). Crystallite size and d-spacing were obtained from Gaussian fits of the main crystalline peaks, corresponding to the (002) reflection for cotton and the (100) reflection for PET.

Quantitative XRD analysis was not performed on polycotton blend samples owing to the near-coincidence of the cellulose (002) and PET (100) reflections at approximately 22.7° 2θ, which precludes independent component deconvolution; polycotton diffractograms are therefore discussed qualitatively only.

3.5.5 X-ray Photoelectron Spectroscopy (XPS)

XPS measurements were carried out on a Kratos AXIS Ultra DLD spectrometer (Al Kα, 1486.7 eV, 100 W). Survey spectra were acquired at 80 eV pass energy (1.0 eV step, 0–1100 eV); high-resolution C 1s, O 1s, N 1s, Ca 2p, and Si 2p spectra at 20 eV pass energy (0.1 eV step). Photoelectrons were collected at 90° take-off angle under ultra-high vacuum (< 1 × 10−9 Torr) over a 300 × 700 μm2 analysis area. Three spatially distinct positions were measured per sample to assess homogeneity; no charging was observed and all positions contributed to the reported averages. Spectra were charge-referenced to the C–O component at 286.5 eV (corresponding to C–C at 284.8 eV) [53]. Six samples were analysed: control samples (Cot-Ctrl, PET-Ctrl, PC-Ctrl), in which fibres were water-soaked prior to refining, and chemically pretreated samples (Cot-NaU, PET-AcA, PC-NaU), in which NaOH/urea or acetic acid pretreatment was applied before refining. All samples were mechanically refining.

The C 1s envelope was fitted with Gaussian–Lorentzian components of equal FWHM at 284.8 eV (C–C), 286.5 eV (C–O), 287.8 eV (C=O/O–C–O), and 289.0 eV (O–C=O) [54]. Samples containing PET required an additional asymmetric aromatic C=C component at ~284.5 eV and a high-binding-energy plasmon satellite. The O 1s region was deconvoluted into components at ~530.7 eV (C=O), ~532.8 eV (C–O), ~534.2 eV (O–H), and ~535.5 eV (H2O).

3.5.6 Rheology

The viscoelastic and flow properties of chemically pretreated and refining polycotton fibre suspensions were characterised using an Anton Paar rheometer equipped with a concentric cylinder geometry (Anton Paar) with a gap of 1 mm, a bob diameter of 26.66 mm, and a profiled bob surface to prevent wall-slip effects. Prior to rheological measurement, refined fibre samples were homogenised using a disintegrator for 10 minutes, followed by Masuko supermasscolloider grinding (Masuko Sangyo, Japan) for 2 hours. Samples were subsequently air-dried for ~72 hours to a dry matter content of approximately 95 wt%. Suspensions were prepared at a consistency of 2 wt% in deionised water, mixed for 10 minutes using a disintegrator, and sonicated for 10 minutes before loading into the geometry. The PC-Ctrl sample was excluded from rheological analysis due to severe measurement instability at 2 wt%, consistent with the absence of any cohesive network structure in the untreated suspension.

Three measurement protocols were carried out sequentially. First, an amplitude sweep was performed at a fixed angular frequency of ω = 10 rad/s, with strain amplitude varied logarithmically from approximately 10^{-4} to 10^{2}%. This was used to identify the linear viscoelastic region (LVR) and determine the plateau storage modulus (G'_0) and loss modulus (G''_0). The loss tangent was calculated as:

$$\tan\delta = \frac{G''}{G'} \quad (5)$$

where tan δ represents the ratio of loss to storage modulus, with G″ as the loss modulus (Pa) and G′ as the storage modulus (Pa). It provides a measure of the relative viscous and elastic contributions of the suspension.

Second, a frequency sweep was performed at a fixed strain amplitude of γ = 0.01% (within the LVR), with angular frequency ω varied from 0.1 to 100 rad/s to characterise the frequency dependence of G′, G″, and complex viscosity (|η*|). The complex viscosity, which combines both elastic and viscous contributions as $|\eta^*| = \sqrt{(G'^2 + G''^2)} / \omega$, was fitted to the oscillatory power law model:

$$|\eta^*| = A \cdot \omega^n \quad (6)$$

where A (Pa·s) is the pre-factor representing complex viscosity at ω = 1 rad/s, and n is the oscillatory power law exponent. A value of n approaching −1 is indicative of a strongly entangled gel network.

Third, a flow sweep was performed under steady shear to determine apparent viscosity (η) as a function of shear rate (γ̇). The apparent viscosity, defined as η = τ / γ̇ where τ is the measured shear stress (Pa), was fitted to the power law constitutive equation:

$$\eta = K \cdot \dot{\gamma}^{n-1} \quad (7)$$

where η is the apparent viscosity (Pa·s), K is the flow consistency index (Pa·sⁿ), γ̇ is the shear rate (s^{-1}), and n is the flow behaviour index. A value of $n < 1$ indicates shear-thinning behaviour, with n approaching 0 for a strongly shear-thinning system.

3.5.7 Turbiscan Stability Analysis

The colloidal stability of chemically pretreated and blended polycotton fibre suspensions was evaluated using a Turbiscan LAB optical analyser (Formulaction, France). Each suspension was prepared at 0.2 wt% in deionised water, hand-shaken for approximately 10 seconds, and sonicated for 10 minutes prior to measurement. A volume of approximately 20 mL was transferred into the cylindrical glass measurement vial, with the acquisition parameters set to a lower detection limit of 0.6 mm and an upper limit of 80 mm. The instrument scans a pulsed near-infrared source (λ = 880 nm) vertically along the vial, recording transmission (T) at 0° at each height position; a decrease in T corresponds to local fibre accumulation and an increase to clarification [55]. The scans were recorded at 1-minute intervals over a total duration of 60 minutes for three samples: PC-Ctrl, PC-NaU, and PC-AcA. The differential transmission was expressed as:

$$\Delta T = K \cdot T(t) - T(t=0) \quad (8)$$

where T(t) represents the transmission at a given time and T(t = 0) corresponds to the initial profile at t=0. This parameter was used to evaluate changes in transmission as a function of both sample height and time.

3.5.8 Foam Preparation and Characterisation

Foam samples were prepared from polycotton fibres subjected to three treatment conditions: water-soaked control (PC-Ctrl), NaOH/urea pretreatment (PC-NaU), and acetic acid pretreatment (PC-AcA). For each condition, 5 g of dry fibres were dispersed in deionised water (total suspension volume 250 mL, fibre consistency

2 wt%) containing 0.1 wt% sodium dodecyl sulfate (SDS) as surfactant. Prior to foaming, 0.1 wt% methylcellulose was added to each suspension to improve foam stability and viscosity. Foams were produced by mechanical agitation and cast into cylindrical moulds, then dried at ambient conditions to constant mass.

Bulk porosity was determined by the ethanol displacement method [56]. Dried foam samples were submerged in absolute ethanol (ρ = 0.789 g cm−3) for 2 h to ensure thorough saturation. After removal, excess surface ethanol was wiped off and the saturated mass recorded. Porosity (φ) was calculated as:

$$\phi\,(\%) = \frac{m_s - m_0}{\rho \times V} \times 100 \qquad (9)$$

where m□ and m0 are the saturated and dry sample masses, respectively, and V is the apparent geometric volume of the sample. Apparent density was calculated as ρapparent = m0 / V, where V was determined from sample dimensions. Both measurements were performed on two replicates per sample, with results reported as mean ± standard deviation, following the procedure described by Abidnejad et al. [56].

Foam microstructure was examined by scanning electron microscopy (SEM) using a Phenom Pure G5 desktop instrument at an accelerating voltage of 5 kV. Foam samples were freeze-dried for 72 h prior to imaging. Cross-sections were prepared by submerging the dried samples in liquid nitrogen for 4 minutes and cutting with a sharp blade to expose the internal structure; the upper portion was discarded and the freshly exposed surface was used for imaging. Samples were sputter-coated with a gold/palladium alloy at 40 mA for 30 s to mitigate charging effects and examined at multiple magnifications.

4. Results and Discussion

This chapter presents the characterization results for cotton, PET, and polycotton (50/50 wt%) fibres subjected to water-soaked control, NaOH/urea (5/12 wt%), and acetic acid (50 wt%) pretreatments, in both unblended and blended states. Results are presented in the following order: water retention value (WRV), attenuated total reflectance Fourier-transform infrared spectroscopy (ATR-FTIR), scanning electron microscopy (SEM), and X-ray diffraction (XRD). Each section reports the response of all three fibre types, followed by a comparative assessment of treatment effects across unblended and blended conditions.

4.1 Water Retention Value (WRV)

The WRV reflects the fibre's capacity to retain water within its inter-fibrillar pore structure following centrifugation, and serves as a sensitive indicator of fibre swelling, accessible pore volume, and the extent of inter-fibrillar network opening [57]. All measured WRV values are presented in figure 4.

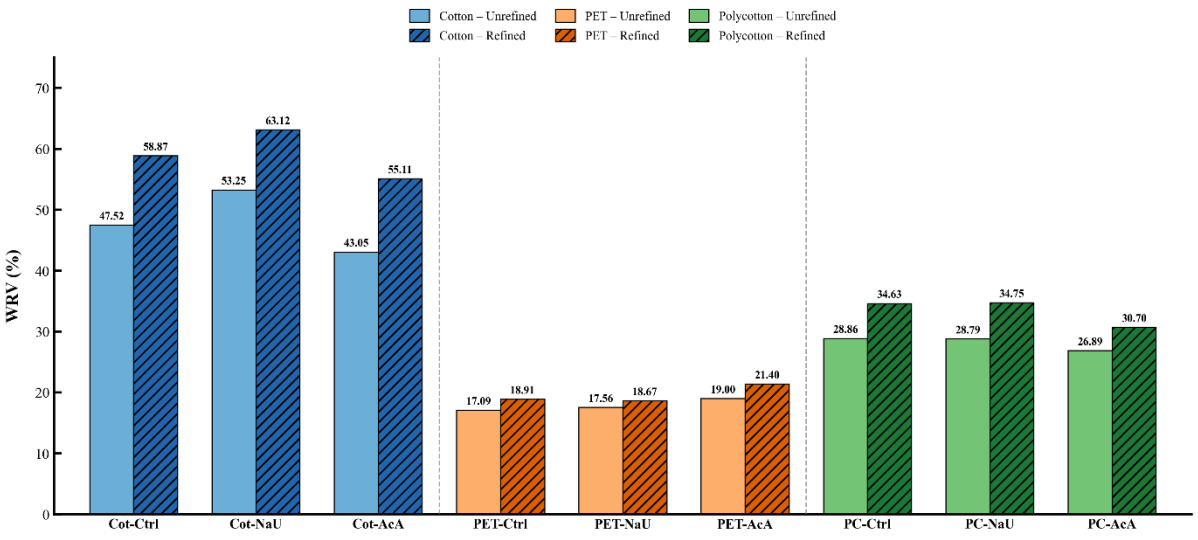

Figure 4: Water retention values (WRV, %) for all fibre types and treatment conditions in unrefined and refined states.

Among the three fibre types, cotton exhibited the highest absolute WRV values across all conditions, consistent with its inherently hydrophilic character and high hydroxyl group density [58]. In the unrefined state, NaOH/urea treatment produced the highest WRV (53.25%), exceeding the control (47.52%) by 12.1%.

This reduction is attributed to two complementary mechanisms. First, at 50 wt% concentration, acetic acid partially dehydrates the inter-chain space and promotes direct cellulose–cellulose hydrogen bonding upon acid removal. This results in irreversible pore closure analogous to acidic hornification [59], [60]. Acetic acid treatment produced a markedly lower WRV (43.05%) compared to the control, representing a decrease of 9.4%. Second, the increase in crystallinity index observed by XRD (from 68.65% in the control to 70.26% after acetic acid treatment) suggests that acid hydrolysis preferentially affects the more accessible amorphous cellulose regions, leaving behind a proportionally higher crystalline fraction. Since amorphous cellulose is mainly responsible for water uptake due to its open structure and higher hydroxyl accessibility, its preferential removal reduces the overall water-holding capacity of the fibre. This effect, together with pore closure, leads to a decrease in WRV [51].

Mechanical refining increased WRV across all samples of cotton regardless of prior treatment, with absolute gains of 23.9% (control), 18.5% (NaOH/urea), and 28.0% (acetic acid) compared to their respective unrefined sample values. The largest refining-induced gain occurred in the acetic acid group, despite its lowest pre-refining WRV, indicating that mechanical shear partially disrupted the consolidated inter-fibrillar bonds formed during acid treatment and re-opened porosity that had been locked by the consolidation process. The NaOH/urea-refined cotton (Cot-NaU-R) recorded the highest WRV across all measurements (63.12%), consistent with a synergistic relationship between alkali pre-swelling and mechanical refining: pre-swelling reduces fibril-fibril cohesion and lowers the threshold mechanical energy for fibrillation, amplifying the surface area gains achievable by refining alone [63].

PET showed negligible WRV response to either treatment, with values ranging from 17.09 to 21.40% across all conditions. The narrow range and absence of directional treatment dependence are consistent with the hydrophobic, chemically inert nature of the polyester backbone under aqueous conditions near room temperature [64].

Polycotton WRV values (26.89-34.75%) fell between the cotton and PET ranges, broadly consistent with a mass-weighted average of the two component fibres. The NaOH/urea treatment produced no measurable WRV change relative

to the control in either the unrefined or refined state, unlike the clear 12.1% gain observed in pure cotton. The suppression of the alkaline swelling response in polycotton likely reflects a combination of factors that are difficult to decouple from the present data. PET s may physically constrain outward cotton swelling, restrict aqueous penetration into the bundle during treatment, and reduce the water retained in inter- capillary spaces — since approximately half of the adjacent surfaces in the blend are hydrophobic PET, the capillary spaces between cotton and PET surfaces would retain considerably less water than those between two swollen cotton s. The relative contribution of each mechanism cannot be conclusively determined, but their combined effect is consistent with the observed suppression of the WRV response in the blend. Acetic acid, however, still reduced polycotton WRV by 6.8% (unrefined) and 11.3% (refined) relative to their respective controls. This partial survival of the acetic acid WRV signal in polycotton — in contrast to the complete suppression of the NaOH/urea response — is consistent with the fundamental difference between the two mechanisms. Alkaline swelling acts outward, expanding the volume, and is therefore susceptible to physical constraint by surrounding PET s. Acid-induced consolidation and amorphous cellulose hydrolysis, however, act within the cotton itself and are not obstructed by adjacent PET s, allowing the WRV reduction to persist even in the refined state.

4.2 ATR-FTIR Spectroscopy

ATR-FTIR spectra were recorded over 4000-500 cm-1 for all samples. Spectra for cotton, PET, and polycotton are presented in Figures 5, 6 and 7 respectively. Key band assignments are summarised in Table 2.

Table 2: Key ATR-FTIR band assignments for cotton, PET, and polycotton fibre samples across all treatment conditions

Wavenumber (cm-1)	Assignment	Fibre type	Treatment dependence
3326	O-H stretching (H-bonded)	Cotton, Polycotton	Present in all; intensity unchanged
2904	C-H stretching (CH2)	Cotton, Polycotton	Unchanged across all conditions
1710	C=O stretching	Cotton	Most intense in NaOH/urea; faint peak in control and acetic acid

1637	O-H bending, adsorbed water	All fibre types	Most prominent in acetic acid cotton
1713	C=O ester carbonyl stretching	PET, Polycotton	Unchanged across all conditions
3430	O-H stretching, surface hydroxyl	PET	Weak band, NaOH/urea-treated only

All cotton spectra retained the characteristic absorption profile of cellulose I across the full measurement range (Figure 5). The O-H stretching band at 3326 cm-1, assigned to intra- and inter-molecular hydrogen-bonded hydroxyl groups, and the C-H stretching band at 2904 cm-1 were present in all three samples with no positional shift, confirming that neither treatment altered the primary cellulosic structure. The significant change was the appearance of a band at 1710 cm^{-1} exclusively in the NaOH/urea-treated cotton spectrum, absent in both control and acetic acid samples. This band is likely due to C=O stretching caused by mild oxidation of cellulose under alkaline conditions [65]. Alternatively, it could also arise from the formation of cellulose carbamate, as urea can react with cellulose in alkaline media to produce a urethane C=O band around 1710 cm^{-1}[66]. No cellulose II marker bands were detected in any cotton sample, confirming retention of the cellulose I polymorph across all treatment conditions used. This is consistent with the sub-mercerising NaOH concentration employed: Ji et al. (2018) [67] established that cellulose I-to-II conversion requires a minimum NaOH concentration of approximately 12 wt%, while concentrations in the 3-6 wt% range selectively disrupt amorphous inter-fibrillar domains without inducing polymorphic transformation [68].The 1637 cm^{-1} band assigned to O–H bending of adsorbed water appeared comparable across both treatment conditions, suggesting no significant difference in moisture affinity between alkaline and acid-treated cotton s relative to the control [68].

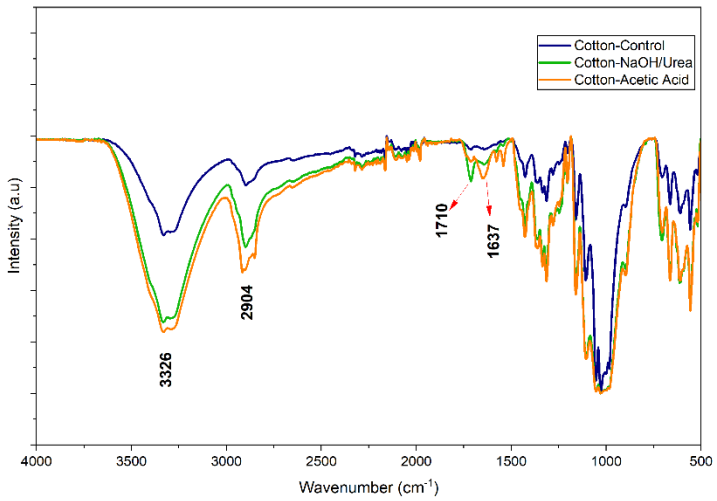

Figure 5: ATR-FTIR spectra of cotton fibres under control, NaOH/urea, and acetic acid treatment conditions recorded over 4000–500 cm^{-1}

PET spectra (Figure 6) were characterised by the ester carbonyl C=O stretching band at 1713 cm^{-1}, C–H stretching at 2962 cm^{-1}, and a broad O–H feature at 3430 cm^{-1}. All three treatment spectra were superimposable across the full range, confirming that neither NaOH/urea nor acetic acid treatment induced any detectable change in PET chemical structure, consistent with the known chemical inertness of polyester under the mild aqueous conditions employed.

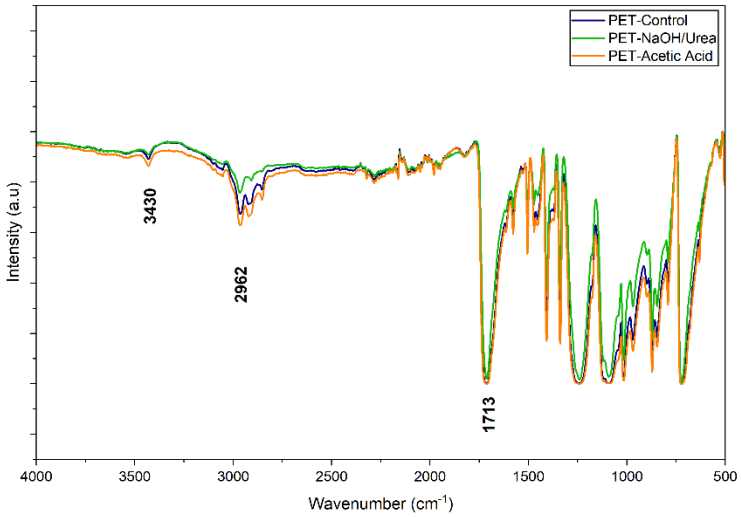

Figure 6: ATR-FTIR spectra of PET fibres under control, NaOH/urea, and acetic acid treatment conditions recorded over 4000–500 cm^{-1}

Polycotton spectra showed the expected superposition of cellulosic and polyester absorption features across all conditions (Figure 7). Treatment-induced spectral differences were subtle overall, with the acetic acid-treated sample showing only slightly distinct features in the O–H stretching region relative to the control. More broadly, the attenuated spectral response of polycotton relative to pure cotton across all treatment conditions is consistent with the WRV data and suggests that the presence of PET s reduces the overall chemical responsiveness of the cotton component within the blend.

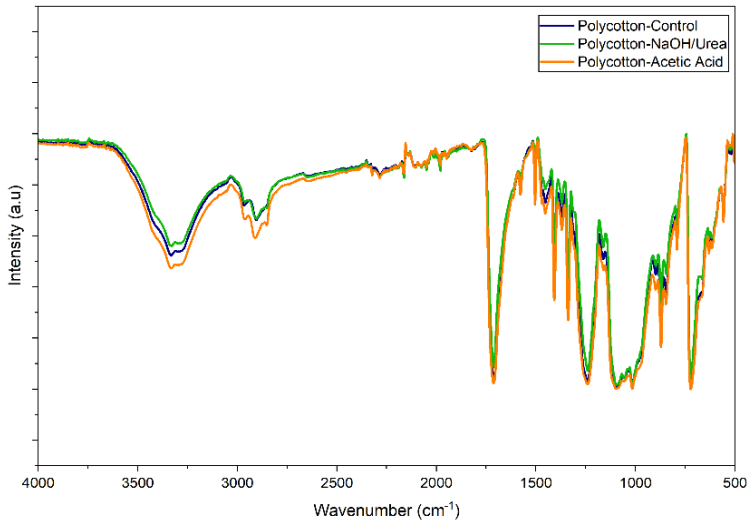

Figure 7: ATR-FTIR spectra of Polycotton fibres under control, NaOH/urea, and acetic acid treatment conditions recorded over 4000–500 cm^{-1}

4.3 Scanning Electron Microscopy

SEM micrographs of all three fibre types under control-unrefined and control-refined conditions are presented in Figure 8 (panels a–f), and under NaOH/urea-refined and acetic acid-refined conditions in Figure 9 (panels g–l), both at 1000× magnification. Higher magnification micrographs for selected samples of morphological significance are presented in Figure 10.

In the Unrefined state (Control samples), all three fibre types displayed intact morphologies representative of their respective structural origins (Figure 8a–c). Cotton fibres exhibited the collapsed ribbon-like cross-section characteristic of mechanically recycled cellulose, with relatively smooth longitudinal surfaces and no evidence of fibrillar separation. PET fibres appeared as smooth, uniform cylinders with featureless surfaces. Polycotton showed the expected mixture of

both morphologies within the same fibre assembly. The refined-control samples (Cot-Ctrl-R, PC-Ctrl-R, and PET-Ctrl-R samples) (Figure 8d–f) showed modest mechanical surface disruption in cotton and polycotton, primarily manifest as minor longitudinal splitting attributable to refining shear, while PET surfaces remained unchanged.

NaOH/urea treatment combined with refining produced the most pronounced morphological changes across the entire dataset (Figure 9g–i). Cotton fibres showed extensive longitudinal fibrillation with individual fibrillar elements delaminating from the fibre surface along the fibre axis; this is resolved in greater detail at 2000× magnification (Figure 10a). The organised, parallel nature of the delaminated fibrils is consistent with preferential alkali attack on inter-fibrillar cementing material rather than the covalent cellulose backbone, which would produce random fragmentation. An analogous delamination morphology has been reported for kraft pulp fibres subjected to alkaline pre-treatment prior to mechanical refining, where alkali-induced inter-fibrillar swelling lowered the mechanical energy threshold for fibril detachment [63]. The extensive fibrillation and increased surface area generated by NaOH/urea treatment and refining are consistent with the highest WRV recorded across all samples (63.12%), as the newly exposed fibrillar surfaces and enlarged inter-fibrillar pore volume directly increase the fibre's capacity to retain water. In the PC-NaU-R sample (Figure 9h), fibres corresponding to the cotton component showed comparable surface fibrillation, while fibres consistent with the PET component retained smooth cylindrical morphologies indistinguishable from the control, confirming the chemical selectivity of the treatment to the cellulosic fraction.

Acetic acid treatment combined with refining produced a morphologically distinct and contrasting outcome (Figure 9j–l). Cotton fibres showed a more compact and consolidated surface with reduced fibrillar separation compared to Cot-NaU-R. Localised surface cracking was also observed, consistent with fibre embrittlement under concentrated acid exposure Figure 9j). In the PC-AcA-R sample, the flat ribbon-like cotton fibres showed a more compacted surface compared to the control, while the cylindrical PET fibres remained unchanged (Figure 9k; detail in Figure 10b). PET fibres exposed to acetic acid showed only minor surface deformation relative to the control but retained their structural integrity across all observed areas (Figure 9l). The compacted and consolidated

surface morphology observed in acetic acid-treated cotton is consistent with the reduced WRV of Cot-AcA (43.05% unrefined, 55.11% refined). This supports the interpretation that acid-induced inter-fibrillar consolidation reduces the fibre's water retention capacity.

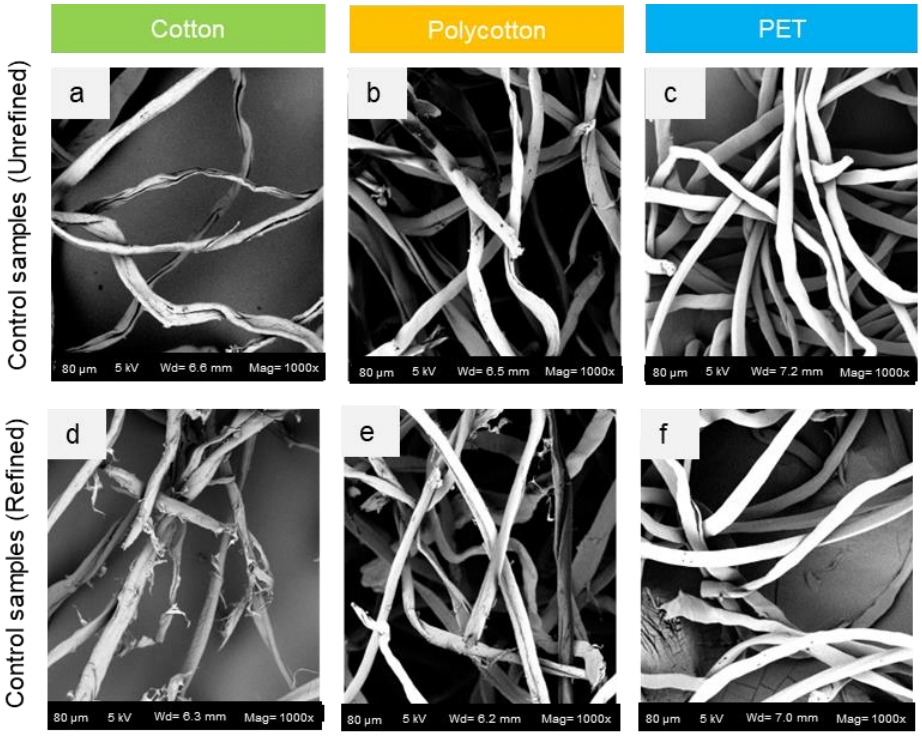

Figure 8: Scanning electron micrographs of unrefined (a–c) and refined (d–f) fibre samples under water control treatment: (a) Cot-Ctrl-UR, (b) PC-Ctrl-UR, (c) PET-Ctrl-UR, (d) Cot-Ctrl-R, (e) PC-Ctrl-R, (f) PET-Ctrl-R.

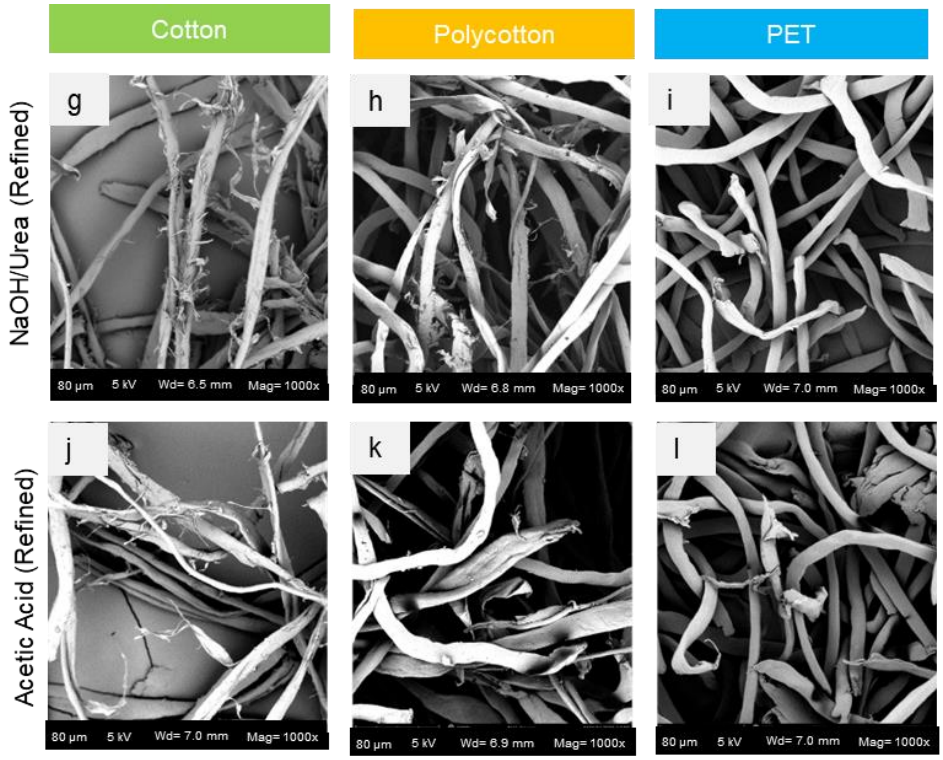

Figure 9: Scanning electron micrographs of refined fibre samples under NaOH/urea (g–i) and acetic acid (j–l) pretreatments: (g) Cot-NaU-R, (h) PC-NaU-R, (i) PET-NaU-R, (j) Cot-AcA-R, (k) PC-AcA-R, (l) PET-AcA-R.

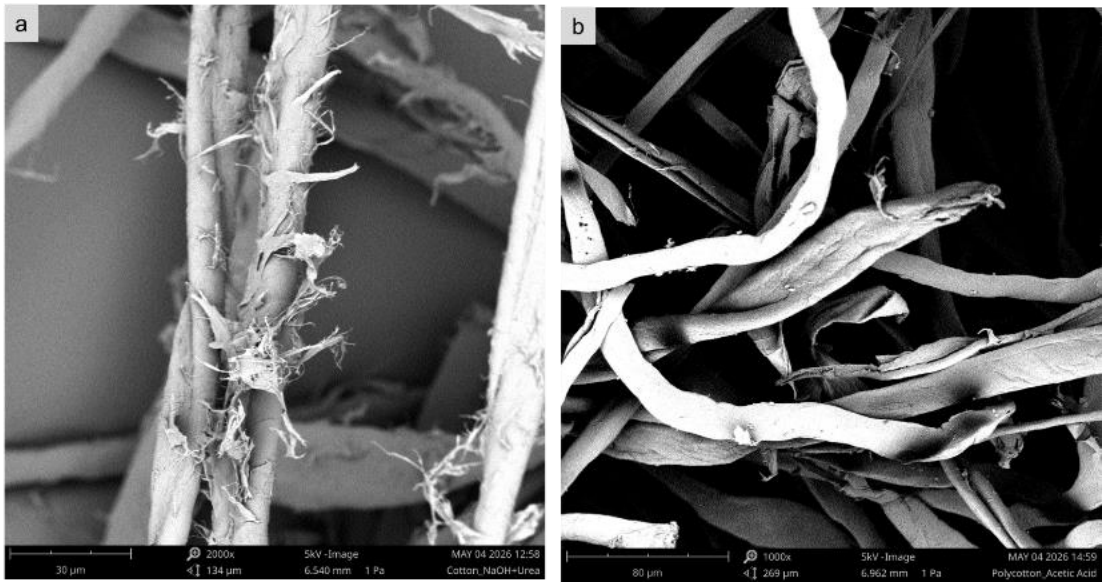

Figure 10: High-magnification SEM micrographs (2000×) of selected samples: (a) Cot-NaU-R showing fibril delamination at the fibre surface; (b) PC-AcA-R

4.4 X-ray Diffraction

Throughout this section, -UR and -R suffixes denote unrefined and refined sample states, respectively. Diffractograms of all six cotton samples displayed reflections characteristic of cellulose I at the following values of 2θ: ($1\bar{1}0$) at ~14.8°, (110) at ~16.4°, (002) at ~22.7°, and (040) at ~34.2 (Figure 11). No cellulose II reflections were detected in any sample, which confirm the retention of the cellulose I polymorph across all treatment conditions and processing states. CI was determined using a four-peak Gaussian deconvolution model comprising the ($1\bar{1}0$), (110), (002), and (040) crystalline reflections together with one broad amorphous Gaussian; all fits achieved $R^2 \geq 0.995$ (figure 12 as an example, Appendix 1). Scherrer L and d-spacing were derived from the (002) reflection. The complete parameter set is presented in Table 3.

In the unrefined state, CI slightly increased from 68.65% (control) to 69.54% (NaOH/urea) and 70.26% (acetic acid). Scherrer L simultaneously decreased from 4.63 nm (control) to 4.48 nm (NaOH/urea, −3.3%) and 4.46 nm (acetic acid, −3.6%). The (002) d-spacing remained approximately similar at 3.94 Å (control), 3.91 Å (NaOH/urea, −0.03 Å) and 3.92 Å (acetic acid, −0.02 Å). FWHM increased from 1.75° (control) to 1.81° and 1.82° for NaOH/urea and acetic acid respectively, consistent with the reduction in L. The measured d_{002} values of 3.91–3.94 Å are consistent with the typical value of approximately 3.9 Å reported for native cellulose I [69] confirming that neither treatment induced a measurable change in the cellulose unit cell dimensions. The modest increase in CI observed for both treatments is consistent with trends reported in the literature for alkaline and acidic pretreatments of cellulosic s: alkaline treatment at sub-mercerising NaOH concentrations has been shown to preferentially dissolve and remove accessible amorphous material, leaving a proportionally more crystalline residue [70], while acid hydrolysis selectively degrades the less ordered amorphous regions, effectively enriching the crystalline fraction — a mechanism that also accounts for the reduced WRV observed in acetic acid-treated cotton, since amorphous cellulose contributes disproportionately to water retention [51].

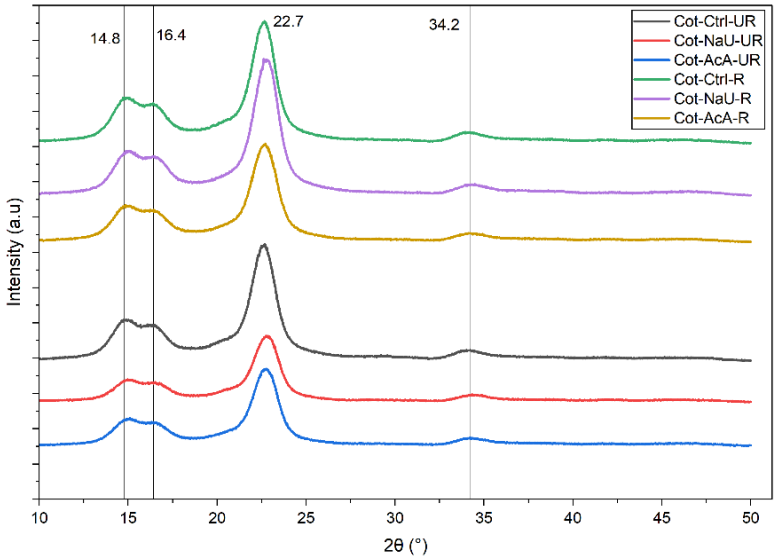

Figure 11: Wide-angle XRD diffractograms of cotton fibres in unrefined and refined states under all three treatment conditions, with characteristic cellulose I reflections at 2θ of ~14.8°, ~16.4°, ~22.7°, and ~34.2°.

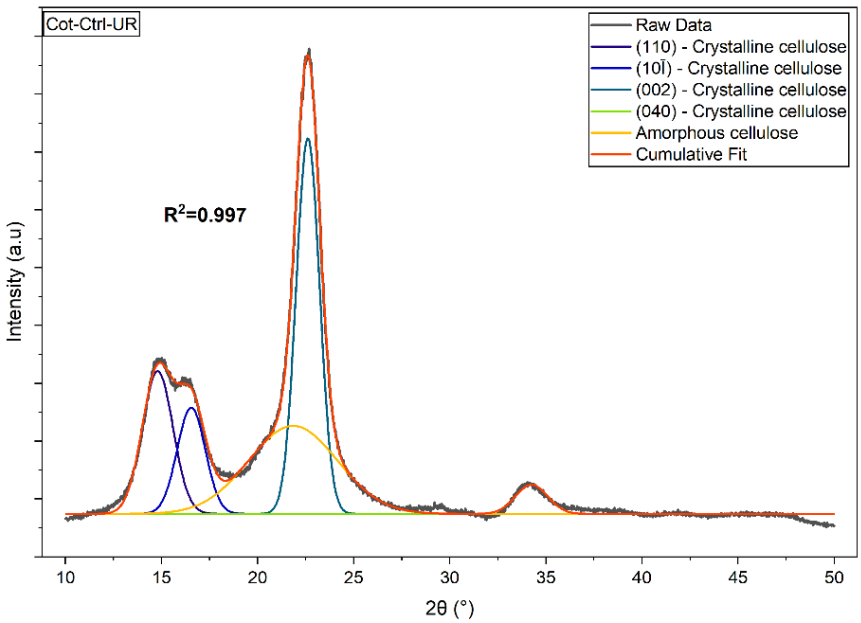

Figure 12; Representative Gaussian deconvolution of the XRD profile for COT-Ctrl-U, showing fitted crystalline peaks (1$\bar{1}$0), (110), (002), and (040) and the amorphous Gaussian component.

Table 3: Table 4.3. XRD parameters for cotton samples: area-based CI from four-peak Gaussian deconvolution, Scherrer crystallite size (L) and d-spacing from the (002) reflection.

Sample	CI (%)	L (nm)	d_{002} (Å)
Cot-Ctrl-UR	68.65	4.63	3.94
Cot-NaU-UR	69.54	4.48	3.91
Cot-AcA-UR	70.26	4.46	3.92
Cot-Ctrl-R	69.38	4.70	3.94
Cot-NaU-R	70.48	4.57	3.91
Cot-AcA-R	70.73	4.42	3.93

In the unrefined state, CI slightly increased from 68.65% (control) to 69.54% (NaOH/urea) and 70.26% (acetic acid). Scherrer L simultaneously decreased from 4.63 nm (control) to 4.48 nm (NaOH/urea, −3.3%) and 4.46 nm (acetic acid, −3.6%). The (002) d-spacing remained approximately similar at 3.94 Å (control) 3.91 Å (NaOH/urea, −0.03 Å) and 3.92 Å (acetic acid, −0.02 Å).

Refining produced divergent effects on L depending on prior treatment. COT-CTR-R (4.70 nm) and COT-NaU-R (4.57 nm) samples both recorded higher L than their respective unrefined counterparts (+0.07 and +0.10 nm respectively), while COT-ACA-R (4.42 nm) recorded a lower value than its unrefined counterpart (−0.04 nm).

Diffractograms of all six PET samples showed three reflections of the triclinic PET unit cell: $(1\bar{1}0)/(010)$ at 2θ of ~17.5°, (110) at ~22.7°, and (100) at ~25.6°, together with a broad amorphous hump centred at ~21° (Figure 13). CI was determined from three-peak Gaussian deconvolution with one amorphous Gaussian component; all fits achieved $R^2 \geq 0.99$ (Figure 14; Appendix 2). Scherrer L was calculated from the (100) reflection using a fitting window of 24.0–27.5° 2θ to account for partial overlap with the adjacent (110) peak tail. Results are presented in Table 4.

Among unbrefined PET samples, CI increased from 34.69% (PET-Ctrl-UR) to 36.33% (PET-NaU-UR) and 37.49% (PET-AcA-UR). L followed the same trend,

increasing from 3.70 nm (PET-CTR-UR) to 3.88 nm (PET-NaU-UR)) and 4.01 nm (PET-AcA-UR). Among refined samples, CI ranged from 35.24% to 37.93%, with PET-NaU-R recording the highest value.

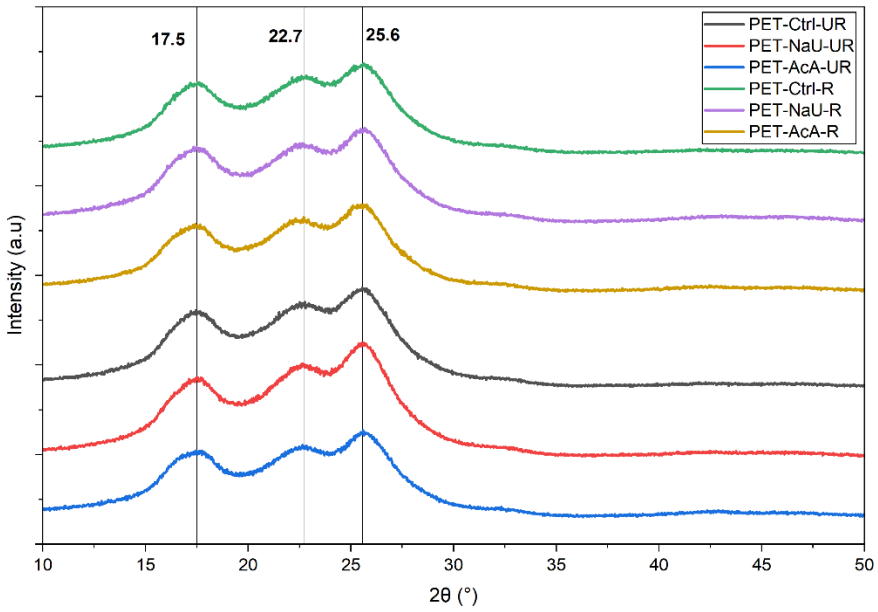

Figure 13: Wide-angle XRD diffractograms of PET fibres in unrefined and refined states under all three treatment conditions, with characteristic triclinic PET reflections at 2θ of ~17.5°, ~22.7°, and ~25.6°.

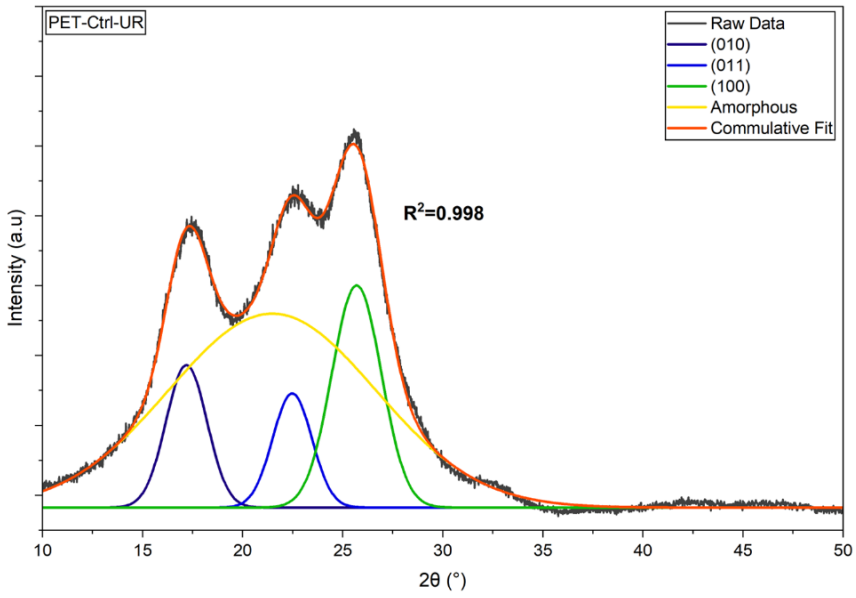

Figure 14: Representative Gaussian deconvolution of the XRD profile for PET-Ctrl-UR, showing fitted crystalline peaks (010), (011), and (100) and the amorphous Gaussian component.

Table 4: XRD parameters for PET samples: area-based CI from three-peak Gaussian deconvolution and Scherrer crystallite size from the (100) reflection (L_{100}).

Sample	CI (%)	L_{100} (nm)
PET-Ctrl-UR	34.69	3.70
PET-NaU-UR	36.33	3.88
PET-AcA-UR	37.49	4.01
PET-Ctrl-R	35.24	3.67
PET-NaU-R	37.93	3.89
PET-AcA-R	37.53	3.89

Polycotton diffractograms showed a superposition of cellulose I and PET reflections across all three treatment conditions (Figure 15). The cellulose ($1\bar{1}0$), (110), and (002) reflections and the PET ($1\bar{1}0$)/(010), (110), and (100) reflections were all identifiable, with the overlapping cellulose (002) and PET (100) contributions producing a broad composite maximum at ~22.5° 2θ that could not be independently resolved. No qualitative differences in peak positions or relative intensities were observed between the different treatment conditions.

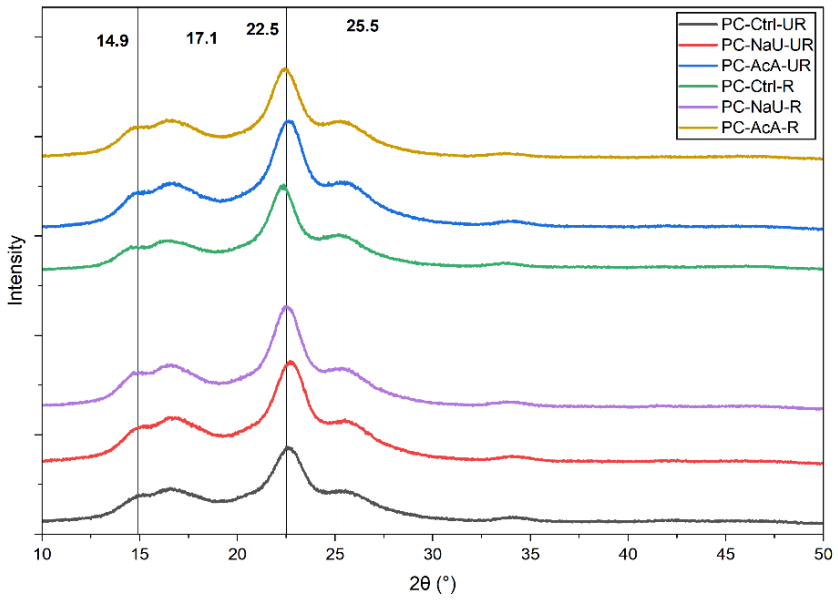

Figure 15: Wide-angle XRD diffractograms of polycotton fibres under all three treatment conditions.

4.5 X-ray Photoelectron Spectroscopy (XPS)

Figure 16 confirmed that carbon and oxygen were the dominant surface elements across all samples. Trace nitrogen, calcium, and silicon were also detected and are addressed briefly below. Elemental compositions and O/C ratios are summarised in Table 5.

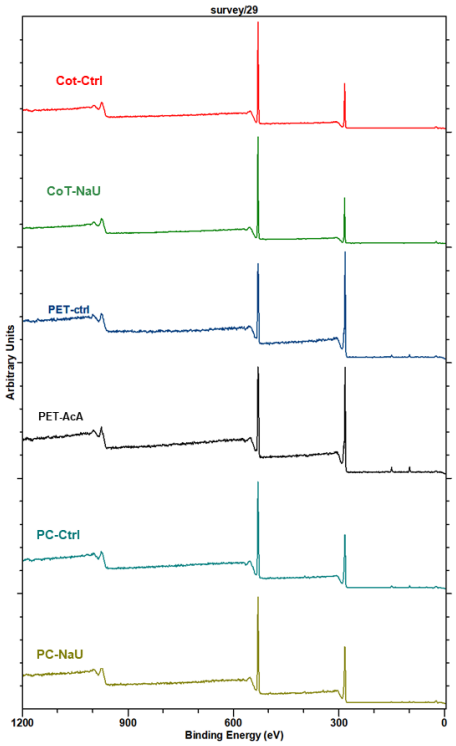

Figure 16: XPS survey spectra of selected refined fibre samples (Cot-Ctrl, Cot-NaU, PET-Ctrl, PET-AcA, PC-Ctrl, and PC-NaU) over the binding energy range 0–1200 eV.

Table 5: Average surface elemental composition and O/C ratio (atomic-%). All samples were mechanically refined.

Sample	C 1s (%)	Ca 2p (%)	N 1s (%)	Na 1s (%)	O 1s (%)	Si 2p (%)	O/C
CoT-Ctrl	63.32	0.15	0.42	0.00	36.11	0.00	0.57
CoT-NaU	61.75	0.02	0.02	0.00	38.20	0.00	0.62
PET-Ctrl	77.00	0.07	0.17	0.00	21.12	1.63	0.27
PET-AcA	74.11	0.04	0.43	0.00	21.89	3.53	0.30
PC-Ctrl	69.49	0.14	0.40	0.00	28.31	1.66	0.41
PC-NaU	69.16	0.14	0.39	0.01	29.64	0.66	0.43

The O/C ratio is the primary indicator of surface cellulose exposure: the theoretical value for pure cellulose $(C_6H_{10}O_5)n$ is 0.83; values below this reflect coverage by hydrocarbon-rich non-cellulosic material [71]. Cot-Ctrl yielded O/C = 0.57, consistent with literature values for cotton bearing residual waxes, fatty acids, and proteinaceous surface constituents [71], [72]. After NaOH/urea pretreatment, CoT-NaU increased to 0.62. This was accompanied by near-complete elimination of surface nitrogen (0.42 → 0.02 at-%) and a reduction in calcium (0.15 → 0.02 at-%). These changes indicate removal of nitrogenous sizing agents and calcium pectate residues from the primary cell wall, leading to greater exposure of the underlying cellulose surface [71], [72].

PET-Ctrl exhibited an O/C ratio of 0.27, reflecting the predominantly aromatic and aliphatic carbon structure of polyethylene terephthalate. PET-AcA showed only a minor change (O/C = 0.30), confirming the chemical inertness of PET under mild acid conditions, consistent with the overlapping ATR-FTIR spectra across PET treatments.

Silicon was not detected in any cotton samples but appeared exclusively in PET-containing samples at a Si 2p binding energy of ~101.9 eV, characteristic of an amorphous silicone-type surface finish [54] commonly applied to PET during manufacturing.

PC-Ctrl showed an intermediate O/C ratio of 0.41, consistent with a 50/50 cotton–PET blend where both fibre types contribute to the surface signal. After NaOH/urea pretreatment, PC-NaU increased only slightly to 0.43, which is much lower than the response observed for pure cotton (Δ = 0.02 vs. 0.05). This weaker response mirrors the reduced WRV in polycotton and is attributed to PET limiting cotton swelling and restricting surface reorganisation within the blend.

C 1s peak-fit spectra (Figure 17a) and component distributions (Table 6) are discussed below.

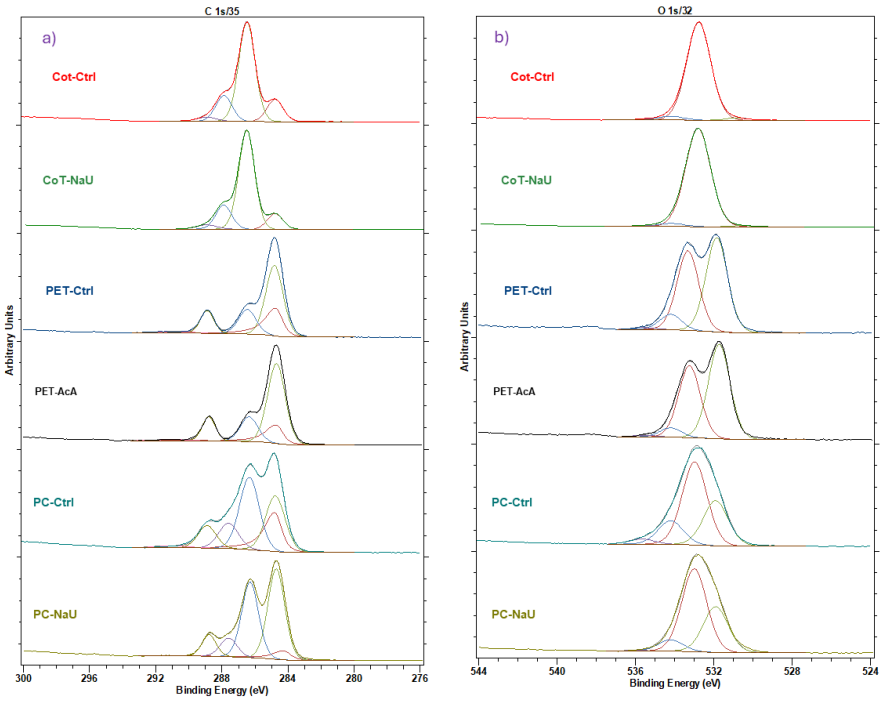

Figure 17: High-resolution XPS (a) C 1s and (b) O 1s peak-fit spectra for all six samples.

Table 6: Relative C 1s component contributions (% of total carbon).

Sample	C=C (%)	C–C (%)	C–O (%)	C=O (%)	O–C=O (%)	Total (%)
Cot-Ctrl	—	16.44	62.80	17.03	3.73	100
Cot-NaU	—	11.51	67.00	17.27	4.21	100
PET-Ctrl	19.51	51.87	16.71	—	11.91	100
PET-AcA	16.35	54.39	17.09	—	12.16	100
PC-Ctrl	18.94	26.27	34.95	10.73	9.12	100
PC-NaU	10.06	32.27	38.15	10.29	9.23	100

The C–O component at 286.5 eV — the dominant chemical environment in the cellulose glucopyranose ring — increased from 62.80% (Cot-Ctrl) to 67.00% (CoT-NaU), while aliphatic C–C fell from 16.44% to 11.51% (Figure 2). This confirms the removal of hydrocarbon-rich non-cellulosic surface material and greater cellulosic backbone exposure following the pretreatment. The C=O and O–C=O components detected in cotton are not inherent to cellulose and are attributed to residual surface contaminants, such as waxes and fatty acids, which remain even after alkaline pretreatment. The slight 1710 cm^{-1} FTIR intensification in Cot-NaU

sample may reflect minor cellulose oxidation, though contamination retention cannot be excluded. PET samples showed a characteristic aromatic C=C component (~19.5 and 16.4% respectively) and dominant aliphatic C–C fraction (~52–54%), consistent with the PET repeat unit and in agreement with the 1713 cm^{-1} ATR-FTIR ester carbonyl band (Section 4.2). Polycotton C 1s profiles were intermediate, with the C–O component increasing modestly from 34.95% (PC-Ctrl) to 38.15% (PC-NaU) — directionally consistent with but considerably smaller than the cotton response.

O 1s peak-fit spectra (Figure 17b) and component distributions (Table 7) are discussed below.

Table 7: Relative O 1s component contributions (% of total oxygen).

Sample	O(C=O) (%)	O(C–O) (%)	O(OH) (%)	O(H_2O) (%)
Cot-Ctrl	2.59	91.77	4.83	0.81
Cot-NaU	1.16	94.37	3.75	0.72
PET-Ctrl	50.04	42.71	6.14	1.11
PET-AcA	53.58	40.17	5.12	1.13
PC-Ctrl	28.03	58.27	11.98	1.73
PC-NaU	28.67	60.62	9.99	0.72

Cotton O 1s spectra were dominated by the C–O single-bond component (91.77% in Cot-Ctrl; 94.37% in CoT-NaU), consistent with the ether- and hydroxyl-rich cellulose backbone. PET samples showed approximately equal O(C=O) and O(C–O) contributions (~50–54% and 40–43% respectively), corresponding to the two oxygen environments of the PET ester group, in agreement with the 1713 cm^{-1} ATR-FTIR absorption. The O(OH) hydroxyl component in polycotton was notably elevated relative to both pure fibre types (PC-Ctrl: 11.98%; PC-NaU: 9.99% vs. ~4–6% for single-component fibres), likely reflecting moisture retention at cotton–PET fibre contacts within the blend, consistent with the slightly broadened 1637 cm^{-1} O–H bending absorption in the polycotton ATR-FTIR spectra.

N 1s spectra (Appendix 5a) showed trace nitrogen at ~399.9 eV (amine-type), markedly reduced in Cot-NaU relative to Cot-Ctrl, confirming alkaline removal of

proteinaceous surface residues. Ca 2p spectra (Appendix 5b) similarly showed ionic Ca^{2+} at ~347.7 eV reduced in Cot-NaU, consistent with removal of calcium pectates.

4.6 Rheological Properties of Polycotton Fibre Suspensions

4.6.1 Amplitude Sweep - Network Strength and Linear Viscoelastic Region

The amplitude sweep profiles for PC-NaU and PC-ACA are presented in Figure 18. Both suspensions exhibited G′ > G″ throughout the LVR, with tan δ = G″/G′ = 0.097 (PC-NaU: G'_0 = 2,970 Pa, G''_0 = 287 Pa) and tan δ = 0.080 (PC-ACA: G'_0 = 454 Pa, G''_0 = 37 Pa), confirming gel-like behaviour in which elastic energy storage dominates over viscous dissipation for both samples. Both G′ and G″ remained constant and strain-independent within the LVR, which extended to approximately 0.040% strain amplitude for PC-AcA.

For PC-NaU, the LVR was slightly broader, extending up to ~0.1% strain, indicating a more robust fibril–fibril network formed under alkaline treatment. This is consistent with the higher G'_0 observed for this sample. Beyond 0.040% strain, G′ decreased progressively as the fibre network was disrupted by deformation. This gel-like response is typical of entangled fibre networks and agrees with behaviour reported for cellulose nanofibril suspensions at comparable or lower concentrations. [73].

The plateau storage modulus differed substantially between treatments, with PC-NaU showing a G'_0 approximately 6.5 times higher than PC-AcA. This aligns with the contrasting fibre morphologies observed by SEM: NaOH/urea treatment produced extensive longitudinal fibrillation of the cotton component, generating finer, elongated fibrils, whereas acetic acid treatment led to surface consolidation and embrittlement, resulting in shorter, stiffer fibre fragments. The lower G'_0 of PC-AcA is attributed to the reduced fibril surface area and contact available for network formation in the acid-treated suspension [74], [75]. It is also noted that air-drying of the refined fibres prior to suspension preparation may have induced partial hornification of the cellulosic fraction [48], [76], which could reduce fibril

accessibility and network strength. As a result, the reported G'₀ values likely represent conservative estimates compared to never-dried fibres.

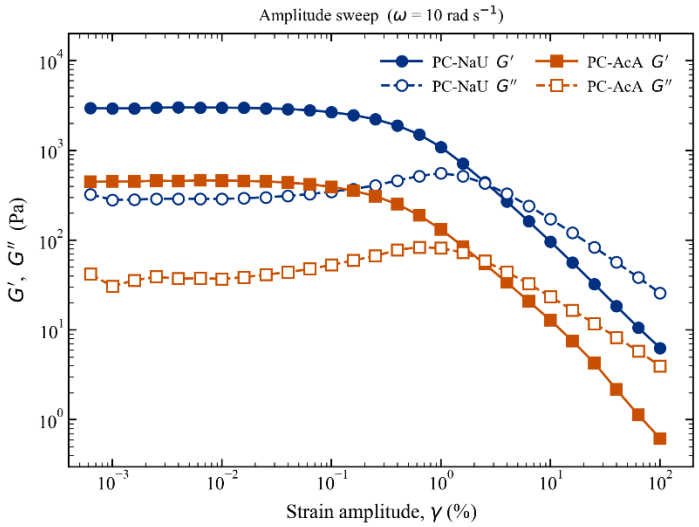

Figure 18: Storage modulus and loss modulus as a function of strain amplitude for PC-NaU and PC-ACA at ω = 10 rad s⁻¹.

4.6.2 Frequency Sweep - Gel Character and Network Relaxation

Both suspensions maintained G' >> G" across 0.1–100 rad/s (Figure 19), with G' showing near-flat frequency dependence: PC-NaU between 2–3 · 10³ Pa and PC-AcA between 1–2 · 10² Pa over the measured window. The absence of a terminal relaxation regime — where G' would decrease steeply at low frequencies for a viscoelastic liquid — confirms that both fibre networks behave as physical gels whose structural relaxation time exceeds the experimental timescale [77].

Power law fitting of |η*| vs ω using Eq. 6 yielded exponents of n = −0.95 for both samples, with pre-factors of A = 2,321 Pa·s (PC-NaU) and A = 125 Pa·s (PC-AcA) (R^2 > 0.999). The n values approach the theoretical limit of n = −1 for a strongly entangled gel, confirming highly entangled network character for both suspensions [74], [77]. The 18.6-fold difference in A is consistent with the substantially stronger network of PC-NaU confirmed by the amplitude sweep. Both suspensions exhibited nearly identical power law exponents (n = −0.95, R^2 > 0.999), suggesting that despite the substantially different network strengths produced by the two pretreatments, the shear-thinning character of the polycotton fibre

suspensions was not significantly affected by the type of chemical pretreatment applied.

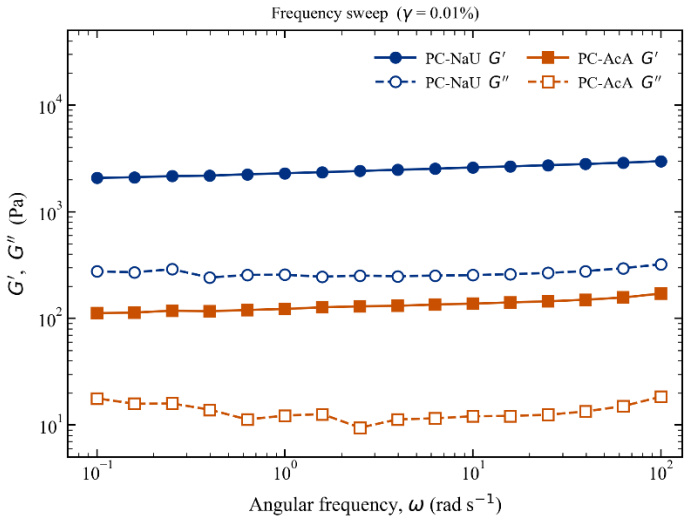

Figure 19: Storage modulus and loss modulus as a function of angular frequency for PC-NaU and PC-ACA at γ = 0.01%.

4.6.3 Flow Sweep - Processability Under Steady Shear

The flow sweep measures apparent viscosity under steady shear (Figure 20), providing insight into suspension behaviour during practical operations such as mixing and casting. Power law fitting using Eq. 3 yielded consistency indices of K = 14.53 Pa·sⁿ (PC-NaU) and K = 1.19 Pa·sⁿ (PC-AcA), with flow behaviour indices of n = 0.10 and n = 0.14 respectively ($R^2 > 0.996$). The 12-fold difference in K shows the higher flow resistance of PC-NaU, consistent with its stronger network formation. Both n values are well below unity and agree with values reported for refining cellulose fibre suspensions at comparable concentrations [78].

The marked deviation of |η*| from η at equivalent frequency and shear rate values constitutes a Cox–Merz rule violation [79] indicating that the fibre network is preserved under gentle oscillatory deformation but broken down under steady shear. This behaviour is practically advantageous — both suspensions resist fibre settling at rest yet flow readily under the shear forces of mixing and casting, which is a desirable property for construction foam applications. Power law fit parameters are provided in Appendix 3.

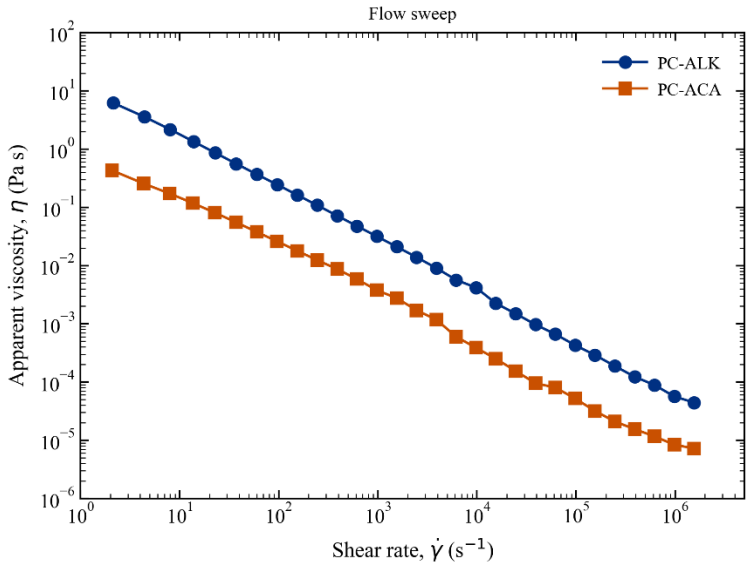

Figure 20: Apparent viscosity (η) as a function of shear rate for PC-NaU and PC-AcA.

4.7 Colloidal Stability of Polycotton Fibre Suspensions

Visual inspection of the three suspensions before Turbiscan analysis gave a simple indication of stability of the suspensions (Figure 21). PC-Ctrl showed complete phase separation into a clear supernatant and a compacted sediment layer, while PC-NaU remained largely turbid throughout with only minimal sedimentation visible at the base. PC-AcA displayed an intermediate state with partial sedimentation and residual turbidity in the upper zone. These observations are directly consistent with the quantitative Turbiscan data presented below.

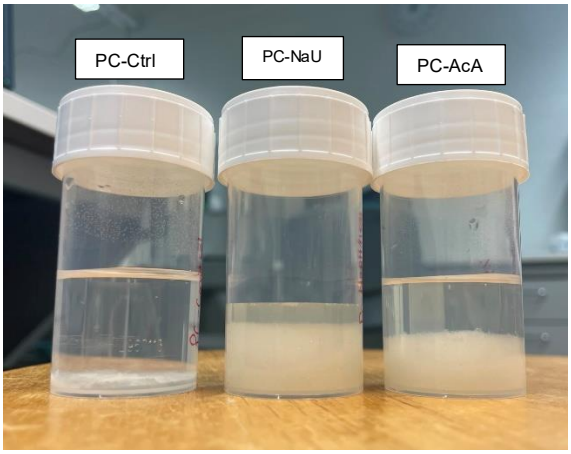

Figure 21. Polycotton fibre suspensions at rest prior to Turbiscan measurement:

4.7.1 Raw Transmission Profiles

The raw transmission profiles as a function of vial height are presented in Figure 22a-c, with height plotted on the vertical axis to reflect the physical orientation of the measurement vial. The t = 0 profile of PC-Ctrl (Figure 22a) showed a non-zero baseline transmission of approximately 40% across the mid-vial region, which indicates that partial sedimentation had occurred during sample transfer and loading prior to the first scan. Despite this, the profiles at t = 10 min onward were fully superimposed with high and uniform transmission across the vial, confirming that sedimentation was effectively complete within the first 10 minutes. The untreated polycotton fibres, having undergone no chemical modification, lack the surface interactions and network-forming capacity necessary to resist gravitational settling, resulting in rapid and irreversible phase separation.

PC-NaU (Figure 22b) exhibited the most distinctive behaviour. A sharp, well-defined clarification front was present in the profiles, migrating progressively from the upper vial toward the base with increasing time. This sharp front — as opposed to a gradual gradient — indicates that the fibre network remained structurally intact below the front while the region above clarified, consistent with coherent network-controlled settling in which the gel yields collectively once the gravitational stress exceeds the network yield stress. At early time points, the lower vial region remained opaque, directly confirming that the entangled fibre network was intact and resisting settling. This behaviour is fully consistent with

the strong viscoelastic gel confirmed by oscillatory rheology (G'₀ = 2,970 Pa, tan δ = 0.097).

PC-ACA (Figure 22c) displayed an intermediate response. A discernible clarification front developed and migrated downward over time, but at a noticeably faster rate and with less structural definition than PC-NaU. This indicates a partially structured suspension that undergoes progressive settling without the coherent network yielding characteristic of the stronger gel, consistent with the weaker viscoelastic network confirmed by rheology (G'₀ = 454 Pa, tan δ = 0.080).

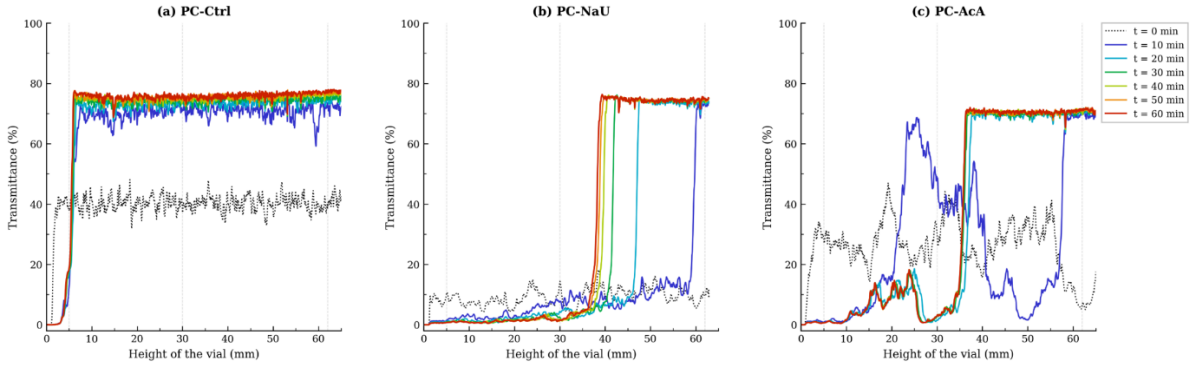

Figure 22: Raw transmission (T) profiles as a function of vial height for (a) PC-Ctrl, (b) PC-NaU, and (c) PC-AcA at selected time points, where Dotted line is initial scan at t = 0 min.

4.7.2 Sedimentation Dynamics at Selected Heights

The ΔT vs time profiles at six representative heights (h = 2, 5, 10, 30, 50, and 62 mm) are presented in Figures 23a–f. At h = 2 mm (Figure 20a), all samples showed negative ΔT, indicating fibre accumulation at the bottom. However, the rates differed strongly between samples. PC-Ctrl reached ΔT ≈ −38% within two scan intervals. PC-AcA stabilised at around −18% within 15 minutes, while PC-NaU showed only ΔT ≈ −9%, consistent with greater fibre retention within the network above the base.

At h = 5 mm (Figure 23b), the trend was similar to that at 2 mm. PC-Ctrl and PC-AcA continued to show fibre accumulation, while PC-NaU remained relatively stable, confirming differences in basal settling behaviour.

At h = 10 mm (Figure 23c), PC-Ctrl quickly developed strong positive ΔT values (~+35%), indicating rapid clarification within 5 minutes. In contrast, PC-NaU stayed close to zero, suggesting that the fibre network maintained a more uniform suspension across the mid-region of the vial.

At h = 30 mm (Figure 23d), PC-Ctrl again showed rapid clarification, whereas PC-NaU remained near zero, consistent with sustained network integrity.

At h = 50 mm (Figure 23e), PC-NaU remained near zero for approximately 17 minutes before transitioning over 2–3 scan intervals to a stable plateau of ΔT ≈ +63%, reflecting the passage of the descending clarification front as the network incrementally yielded under sustained gravitational loading. At h = 62 mm (Figure 23f), all samples eventually clarified, with onset times of less than 1 minute (PC-Ctrl), within the first few minutes (PC-AcA), and approximately 10 minutes (PC-NaU), confirming the overall stability ranking across the full vial height.

The Turbiscan data establish a consistent stability ranking of PC-NaU > PC-ACA > PC-CTR, in full agreement with the rheological results. The convergence of optical stability and rheological data confirms that NaOH/urea pretreatment promotes a fibre entanglement network sufficiently robust to delay gravitational destabilisation — a property directly relevant to construction foam applications where uniform fibre distribution during processing governs final product homogeneity. Supporting ΔT vs height profiles are provided in Appendix 4.

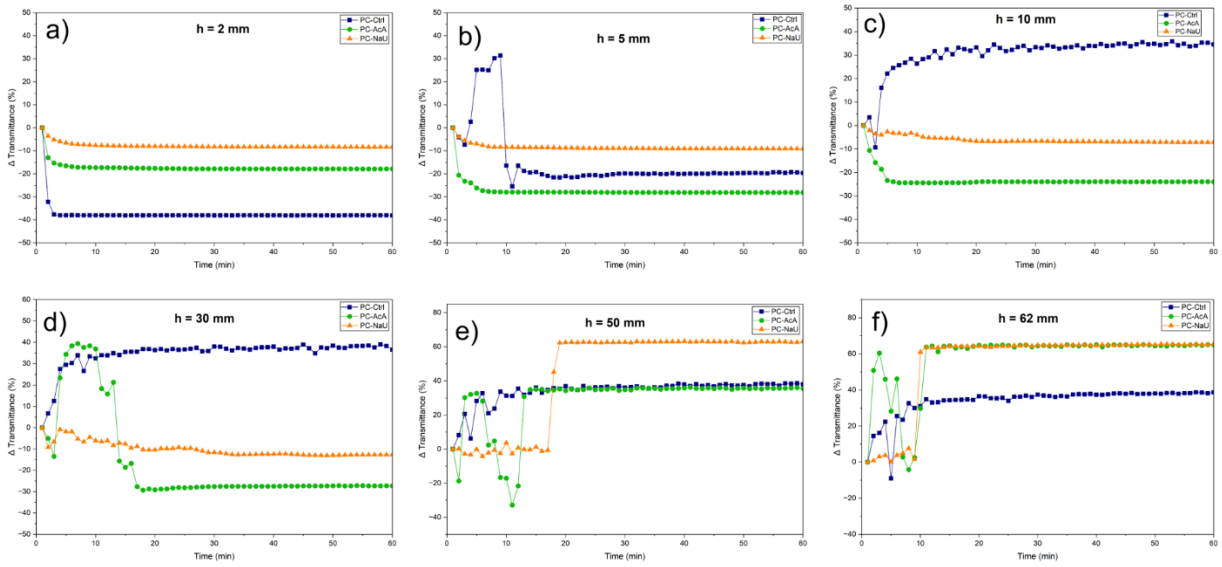

Figure 23: Differential transmittance (ΔT = T(t) − T(t = 0), %) as a function of time at six representative vial heights for PC-Ctrll, PC-NaU and PC-AcA.

4.8 Foam Formation and Physical Characterisation

Foams were prepared from the three pretreated and refined polycotton fibre suspensions by mechanical agitation in the presence of SDS as surfactant, followed by casting into cylindrical moulds and drying at ambient conditions. All three foams were self-standing, lightweight disc structures (Figure 24). PC-Ctrl had the most open and fibrous appearance, while PC-NaU and PC-AcA appeared more consolidated, consistent with the quantitative measurements below.

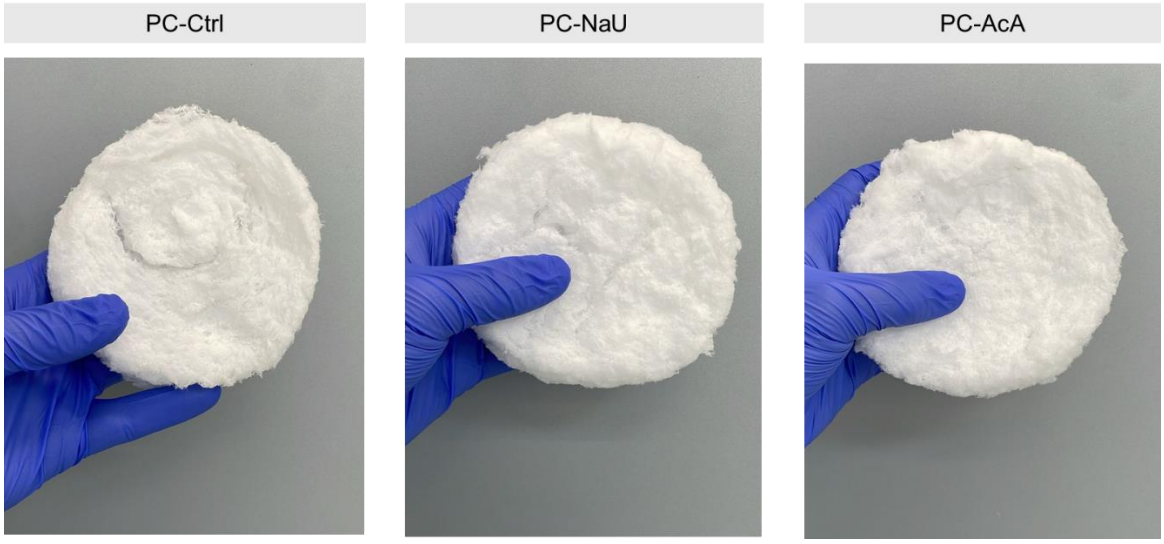

Figure 24: Photographs of polycotton foam discs prepared from water-soaked control (PC-CTR), NaOH/urea pretreated (PC-NaU), and acetic acid pretreated (PC-ACA) fibres.

Bulk porosity decreased from 67.56 ± 0.01% (PC-CTR) to 60.07 ± 0.29% (PC-NaU) and 57.43 ± 0.75% (PC-ACA) (Figure 25a), consistent with the progressive blocking of pore space by fibrillar material observed in SEM (Figure 3). Apparent density ranged from 7.13 to 8.71 kg m^{-3} across the three samples (Figure 25b), with no systematic trend with treatment identified.

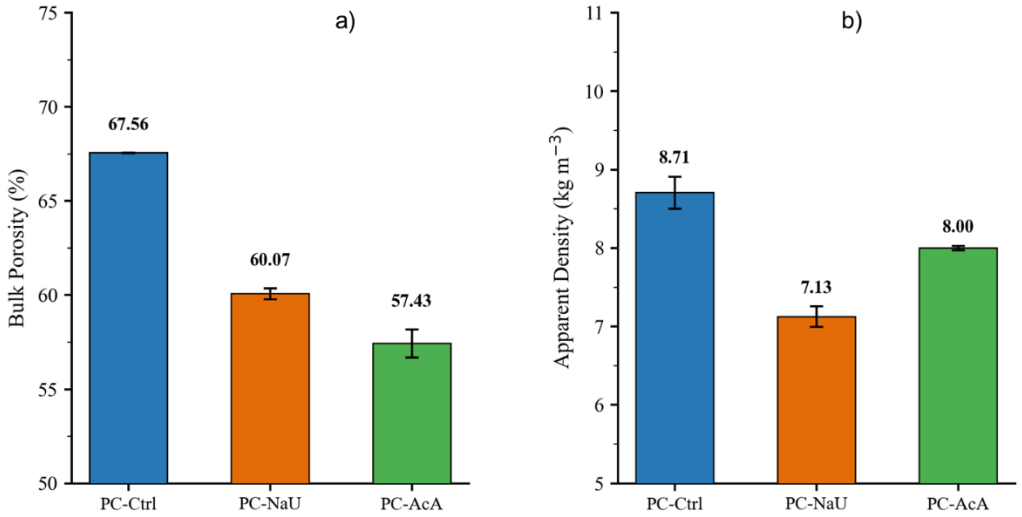

Figure 25: Bulk porosity (a) and apparent density (b) of PC-CTR, PC-NaU, and PC-ACA foams. Error bars represent standard deviation of two replicates.

SEM cross-sections (Figure 26a-c) confirmed that the fibre morphologies established during pretreatment and refining are preserved within the foam structure. PC-Ctrl (Figure 26a) displayed a coarse, open network of smooth PET rods and ribbon-like cotton fibres with large visible voids, consistent with its highest measured porosity. PC-NaU showed abundant fibrils filling the inter-fibre space in a dispersed network formation, in marked contrast to the open voids of PC-Ctrl, confirming that NaOH/urea-induced fibrillation is preserved within the foam structure. PC-AcA (Figure 26c) exhibited moderate fibrillation with partial blocking of inter-fibre pore space, consistent with the acid-induced surface consolidation reported previously.

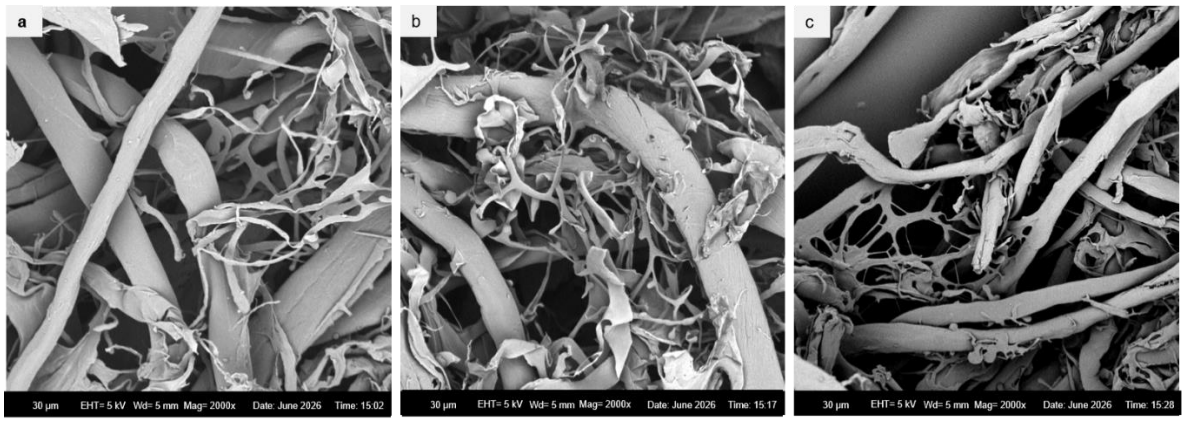

Figure 26: SEM cross-sections of PC-Ctrl (a), PC-NaU (b), and PC-AcA (c) foam structures.

Conclusion

Chemical pretreatment type fundamentally determines the fibrillation pathway and surface chemical response of recycled cotton fibres. NaOH/urea pretreatment induced inter-fibrillar swelling and surface purification in pure cotton, increasing WRV by 12.1% relative to Cot-Ctrl (47.52 to 53.25%) and generating extensive longitudinal fibril delamination upon mechanical refining, as confirmed by SEM. XPS analysis showed near-complete removal of nitrogenous surface contaminants and an increase in the O/C ratio from 0.57 to 0.62, confirming greater cellulose surface exposure. ATR-FTIR revealed a carbonyl band at 1710 cm^{-1} present as a faint peak across all cotton samples but markedly intensified in Cot-NaU, attributed to mild alkaline cellulose oxidation or partial carbamate formation; its persistence in Cot-Ctrl and Cot-AcA is consistent with residual surface contaminants not fully removed by either treatment. The cellulose I polymorph was retained throughout. Acetic acid treatment produced a mechanistically contrasting outcome: WRV decreased by 9.4% to 43.05%, SEM revealed a compacted and consolidated fibre surface, and XRD indicated a higher crystallinity index (70.26% vs. 68.65% for Cot-Ctrl), consistent with selective acid hydrolysis of amorphous cellulose regions. PET fibres were chemically inert under both conditions, showing negligible WRV variation and superimposable spectral and surface elemental profiles across all treatments.

In polycotton suspensions at 2 wt%, PC-NaU produced a substantially stronger viscoelastic gel network (G'_0 = 2,970 Pa) than PC-AcA (G'_0 = 454 Pa), directly reflecting the contrasting fibre morphologies generated by the two treatments: fibrillar entanglement following alkaline fibrillation versus reduced inter-fibre contact following acid-induced consolidation. PC-Ctrl showed no measurable gel-like network and failed to maintain structural stability under measurement conditions, underscoring that chemical pretreatment is indispensable for generating the inter-fibre connectivity required for foam processing. Both treated suspensions exhibited strongly shear-thinning behaviour ($n \approx -0.95$) and Cox–Merz rule violations, confirming physical gel character with practical processability under shear. Turbiscan optical analysis established a sedimentation resistance ranking of PC-NaU > PC-AcA > PC-Ctrl, in full agreement with the rheological data. Across all characterisation methods, the treatment responses of the cotton

component were consistently attenuated in polycotton compared to pure cotton, attributed to physical constraint by PET fibres restricting outward cotton swelling, reduced capillary water retention at cotton–PET interfaces, and limited reagent penetration into the refined fibre bundle. Polycotton foams produced from PC-NaU showed an extensive fibrillar network filling the inter-fibre space and lower bulk porosity (60.07%) compared to PC-Ctrl (67.56%), consistent with improved inter-fibre network consolidation during drying.

These results establish NaOH/urea pretreatment-assisted refining as the more effective strategy for promoting fibrillation, gel network formation, and suspension stability in recycled polycotton fibres, while identifying the dampening effect of PET on cotton fibre reactivity as a fundamental challenge in processing mixed textile streams. Future work should address the mechanical performance of the resulting foam structures under compressive loading, the influence of fibre length distribution on network formation efficiency, and the potential of incorporating reinforcing additives such as cellulose nanocrystals, mineral fillers, or bio-based binders to enhance the stiffness, strength, and dimensional stability of the foam matrix. Optimising fibre-to-additive ratios and exploring surface compatibilisation strategies for cotton–PET interfaces may further improve the homogeneity and functional performance of foams derived from mixed textile waste.

References

[1] "A New Textiles Economy - Redesigning fashions future."

[2] L. Mullen and K. Huun, "A sustainable guide to thrifting | Environmental Center | University of Colorado Boulder." Accessed: Mar. 28, 2026. [Online]. Available: https://www.colorado.edu/ecenter/2023/12/15/sustainable-guide-thrifting

[3] M. D. Stanescu, "State of the art of post-consumer textile waste upcycling to reach the zero waste milestone," *Environ. Sci. Pollut. Res.*, vol. 28, no. 12, pp. 14253–14270, Mar. 2021, doi: 10.1007/s11356-021-12416-9.

[4] Ellen MacArthur Foundation, *A New Textiles Economy: Redesigning Fashion's Future*, vol. 01. Ellen MacArthur Foundation, 2017. [Online]. Available: https://www.ellenmacarthurfoundation.org/a-new-textiles-economy

[5] R. G. Duggleby and H. Kaplan, "A competitive labeling method for the determination of the chemical properties of solitary functional groups in proteins," *Biochemistry*, vol. 14, no. 23, pp. 5168–5175, Nov. 1975, doi: 10.1021/bi00694a023.

[6] S. Kasavan, S. Yusoff, N. C. Guan, N. S. K. Zaman, and M. F. R. Fakri, "Global trends of textile waste research from 2005 to 2020 using bibliometric analysis," *Environ. Sci. Pollut. Res.*, vol. 28, no. 33, pp. 44780–44794, Sep. 2021, doi: 10.1007/s11356-021-15303-5.

[7] "Making Climate Change Fashionable - The Garment Industry Takes On Global Warming." Accessed: Mar. 28, 2026. [Online]. Available: https://www.forbes.com/sites/jamesconca/2015/12/03/making-

climate-change-fashionable-the-garment-industry-takes-on-global-warming/?sh=2d7b6d6179e4

[8] S. Biyada and J. Urbonavičius, "Circularity in textile waste: Challenges and pathways to sustainability," *Clean. Eng. Technol.*, vol. 24, p. 100905, Feb. 2025, doi: 10.1016/j.clet.2025.100905.

[9] M. Schmutz and C. Som, "Identifying the potential for circularity of industrial textile waste generated within Swiss companies," *Resour. Conserv. Recycl.*, vol. 182, p. 106132, Jul. 2022, doi: 10.1016/j.resconrec.2021.106132.

[10] G. Sandin and G. M. Peters, "Environmental impact of textile reuse and recycling – A review," *J. Clean. Prod.*, vol. 184, pp. 353–365, May 2018, doi: 10.1016/j.jclepro.2018.02.266.

[11] M. Koszewska, "Circular Economy — Challenges for the Textile and Clothing Industry," *Autex Res. J.*, vol. 18, no. 4, pp. 337–347, Dec. 2018, doi: 10.1515/aut-2018-0023.

[12] D. Damayanti, L. A. Wulandari, A. Bagaskoro, A. Rianjanu, and H.-S. Wu, "Possibility Routes for Textile Recycling Technology," *Polymers*, vol. 13, no. 21, p. 3834, Nov. 2021, doi: 10.3390/polym13213834.

[13] A. C. Silva *et al.*, "Fibre-to-Fibre Recycling in Textiles: Strategies, Limitations and Industrial Perspectives," *Textiles*, vol. 6, no. 1, p. 30, Mar. 2026, doi: 10.3390/textiles6010030.

[14] K. Shirvanimoghaddam, B. Motamed, S. Ramakrishna, and M. Naebe, "Death by waste: Fashion and textile circular economy case," *Sci. Total Environ.*, vol. 718, p. 137317, May 2020, doi: 10.1016/j.scitotenv.2020.137317.

[15] B. Piribauer and A. Bartl, "Textile recycling processes, state of the art and current developments: A mini review," *Waste Manag. Res. J. Sustain. Circ. Econ.*, vol. 37, no. 2, pp. 112–119, Feb. 2019, doi: 10.1177/0734242X18819277.

[16] M. Kahoush and N. Kadi, "Towards sustainable textile sector: Fractionation and separation of cotton/ polyester fibers from blended textile waste," *Sustain. Mater. Technol.*, vol. 34, p. e00513, Dec. 2022, doi: 10.1016/j.susmat.2022.e00513.

[17] A. D. French and H. J. Kim, "Cotton Fiber Structure," in *Cotton Fiber: Physics, Chemistry and Biology*, D. D. Fang, Ed., Cham: Springer International Publishing, 2018, pp. 13–39. doi: 10.1007/978-3-030-00871-0_2.

[18] A. T. Moore, L. W. Scott, I. V. deGruy, and M. L. Rollins, "The Swelling of Cotton in Water: A Microscopical Study," *Text. Res. J.*, vol. 20, no. 9, pp. 620–630, Sep. 1950, doi: 10.1177/004051755002000904.

[19] M. Mahbubul Bashar and M. A. Khan, "An Overview on Surface Modification of Cotton Fiber for Apparel Use," *J. Polym. Environ.*, vol. 21, no. 1, pp. 181–190, Mar. 2013, doi: 10.1007/s10924-012-0476-8.

[20] C. Fu *et al.*, "Crucial role of fiber swelling in microfibrillated cellulose extraction via ball milling," *Ind. Crops Prod.*, vol. 218, p. 118899, Oct. 2024, doi: 10.1016/j.indcrop.2024.118899.

[21] R. Guru, A. Kumar, J. Rani, R. Fangueiro, S. Panigrahi, and S. Santhanam, "Perspective Chapter: Functional Applications in Textile Reuse and Recycling – Enhancing Sustainability and Reducing Environmental Impact," in *Textile Industry and the Environment* -

Challenges, Recent Development and Future, C. Hui, Ed., IntechOpen, 2025. doi: 10.5772/intechopen.1007986.

[22] M. S. Anas, M. Faheem, and D. Mikucioniene, "Challenges and Limitations in Recycling of Post-Consumer Cotton Denim Waste into New Textiles," *J. Nat. Fibers*, vol. 22, no. 1, p. 2570080, Dec. 2025, doi: 10.1080/15440478.2025.2570080.

[23] H. Zhu *et al.*, "Anomalous scaling law of strength and toughness of cellulose nanopaper," *Proc. Natl. Acad. Sci.*, vol. 112, no. 29, pp. 8971–8976, Jul. 2015, doi: 10.1073/pnas.1502870112.

[24] M. L. Di Lorenzo, "Crystallization of Poly(ethylene terephthalate): A Review," *Polymers*, vol. 16, no. 14, p. 1975, Jul. 2024, doi: 10.3390/polym16141975.

[25] G. Gryn'ova, J. L. Hodgson, and M. L. Coote, "Revising the mechanism of polymer autooxidation," *Org Biomol Chem*, vol. 9, no. 2, pp. 480–490, 2011, doi: 10.1039/C0OB00596G.

[26] V. D. Neelalochana, P. Scardi, and N. Ataollahi, "Polyethylene terephthalate (PET) waste in electrochemical applications," *J. Environ. Chem. Eng.*, vol. 13, no. 3, p. 116823, Jun. 2025, doi: 10.1016/j.jece.2025.116823.

[27] S. Jasmee, G. Omar, N. A. B. Masripan, A. A. Kamarolzaman, A. S. Ashikin, and F. Che Ani, "Hydrophobicity performance of polyethylene terephthalate (PET) and thermoplastic polyurethane (TPU) with thermal effect," *Mater. Res. Express*, vol. 5, no. 9, p. 096304, Aug. 2018, doi: 10.1088/2053-1591/aad81e.

[28] F. Awaja and D. Pavel, "Recycling of PET," *Eur. Polym. J.*, vol. 41, no. 7, pp. 1453–1477, Jul. 2005, doi: 10.1016/j.eurpolymj.2005.02.005.

[29] R. B. Baloyi, O. J. Gbadeyan, B. Sithole, and V. Chunilall, "Recent advances in recycling technologies for waste textile fabrics: a review," *Text. Res. J.*, vol. 94, no. 3–4, pp. 508–529, Feb. 2024, doi: 10.1177/00405175231210239.

[30] J. Liu and X. Peng, "Interface-engineering of the Catalysts for Efficient Electrocatalytic Upcycling of Polyethylene Terephthalate Waste," *Innov. Discov.*, vol. 1, no. 1, p. 1, Mar. 2024, doi: 10.53964/id.2024001.

[31] A. Palme, A. Peterson, H. De La Motte, H. Theliander, and H. Brelid, "Development of an efficient route for combined recycling of PET and cotton from mixed fabrics," *Text. Cloth. Sustain.*, vol. 3, no. 1, p. 4, Dec. 2017, doi: 10.1186/s40689-017-0026-9.

[32] B. Piribauer, A. Bartl, and W. Ipsmiller, "Enzymatic textile recycling – best practices and outlook," *Waste Manag. Res. J. Sustain. Circ. Econ.*, vol. 39, no. 10, pp. 1277–1290, Oct. 2021, doi: 10.1177/0734242X211029167.

[33] K. Choudhury, M. Tsianou, and P. Alexandridis, "Recycling of Blended Fabrics for a Circular Economy of Textiles: Separation of Cotton, Polyester, and Elastane Fibers," *Sustainability*, vol. 16, no. 14, p. 6206, Jul. 2024, doi: 10.3390/su16146206.

[34] P. Harmsen, M. Scheffer, and H. Bos, "Textiles for Circular Fashion: The Logic behind Recycling Options," *Sustainability*, vol. 13, no. 17, p. 9714, Aug. 2021, doi: 10.3390/su13179714.

[35] R. B. Baloyi, O. J. Gbadeyan, B. Sithole, and V. Chunilall, "Recent advances in recycling technologies for waste textile fabrics: a review," *Text. Res. J.*, vol. 94, no. 3–4, pp. 508–529, Feb. 2024, doi: 10.1177/00405175231210239.

[36] K. Lindström, T. Sjöblom, A. Persson, and N. Kadi, "Improving Mechanical Textile Recycling by Lubricant Pre-Treatment to Mitigate Length Loss of Fibers," *Sustainability*, vol. 12, no. 20, p. 8706, Oct. 2020, doi: 10.3390/su12208706.

[37] L. Johansson, "On the Mechanical Recycling of Woven Fabrics".

[38] S.-L. Loo, E. Yu, and X. Hu, "Tackling critical challenges in textile circularity: A review on strategies for recycling cellulose and polyester from blended fabrics," *J. Environ. Chem. Eng.*, vol. 11, no. 5, p. 110482, Oct. 2023, doi: 10.1016/j.jece.2023.110482.

[39] A. Palme, A. Peterson, H. De La Motte, H. Theliander, and H. Brelid, "Development of an efficient route for combined recycling of PET and cotton from mixed fabrics," *Text. Cloth. Sustain.*, vol. 3, no. 1, p. 4, Dec. 2017, doi: 10.1186/s40689-017-0026-9.

[40] E. C. Bensah and M. Mensah, "Chemical Pretreatment Methods for the Production of Cellulosic Ethanol: Technologies and Innovations," *Int. J. Chem. Eng.*, vol. 2013, pp. 1–21, 2013, doi: 10.1155/2013/719607.

[41] N. Mosier, "Features of promising technologies for pretreatment of lignocellulosic biomass," *Bioresour. Technol.*, vol. 96, no. 6, pp. 673–686, Apr. 2005, doi: 10.1016/j.biortech.2004.06.025.

[42] S. Zhang, F. Li, J. Yu, and L. Gu, "Novel fibers prepared from cellulose in NaOH/thiourea/urea aqueous solution," *Fibers Polym.*, vol. 10, no. 1, pp. 34–39, Feb. 2009, doi: 10.1007/s12221-009-0034-8.

[43] Q. Zhou, L. Zhang, M. Li, X. Wu, and G. Cheng, "Homogeneous hydroxyethylation of cellulose in NaOH/urea aqueous solution," *Polym. Bull.*, vol. 53, no. 4, pp. 243–248, Feb. 2005, doi: 10.1007/s00289-005-0334-0.

[44] R. López-Fonseca, M. P. González-Marcos, J. R. González-Velasco, and J. I. Gutiérrez-Ortiz, "A kinetic study of the depolymerisation of poly(ethylene terephthalate) by phase transfer catalysed alkaline hydrolysis," *J. Chem. Technol. Biotechnol.*, vol. 84, no. 1, pp. 92–99, Jan. 2009, doi: 10.1002/jctb.2011.

[45] V. A. Kosmidis, D. S. Achilias, and G. P. Karayannidis, "Poly(ethylene terephthalate) Recycling and Recovery of Pure Terephthalic Acid. Kinetics of a Phase Transfer Catalyzed Alkaline Hydrolysis," *Macromol. Mater. Eng.*, vol. 286, no. 10, p. 640, Oct. 2001, doi: 10.1002/1439-2054(20011001)286:10<640::AID-MAME640>3.0.CO;2-1.

[46] T. Keskin, H. Nalakath Abubackar, K. Arslan, and N. Azbar, "Biohydrogen Production From Solid Wastes," in *Biohydrogen*, Elsevier, 2019, pp. 321–346. doi: 10.1016/B978-0-444-64203-5.00012-5.

[47] A. Jeihanipour and M. J. Taherzadeh, "Ethanol production from cotton-based waste textiles," *Bioresour. Technol.*, vol. 100, no. 2, pp. 1007–1010, Jan. 2009, doi: 10.1016/j.biortech.2008.07.020.

[48] J. M. B. Fernandes Diniz, M. H. Gil, and J. A. A. M. Castro, "Hornification?its origin and interpretation in wood pulps," *Wood Sci. Technol.*, vol. 37, no. 6, pp. 489–494, Apr. 2004, doi: 10.1007/s00226-003-0216-2.

[49] U. Weise, T. Maloney, and H. Paulapuro, "Quantification of water in different states of interaction with wood pulp fibres," *Cellulose*, vol. 3, no. 1, pp. 189–202, Dec. 1996, doi: 10.1007/BF02228801.

[50] Y. Peng, J. Yang, C. Deng, J. Deng, L. Shen, and Y. Fu, "Acetolysis of waste polyethylene terephthalate for upcycling and life-cycle

assessment study," *Nat. Commun.*, vol. 14, no. 1, p. 3249, Jun. 2023, doi: 10.1038/s41467-023-38998-1.

[51] A. D. French and M. Santiago Cintrón, "Cellulose polymorphy, crystallite size, and the Segal Crystallinity Index," *Cellulose*, vol. 20, no. 1, pp. 583–588, Feb. 2013, doi: 10.1007/s10570-012-9833-y.

[52] S. Park, J. O. Baker, M. E. Himmel, P. A. Parilla, and D. K. Johnson, "Cellulose crystallinity index: measurement techniques and their impact on interpreting cellulase performance," *Biotechnol. Biofuels*, vol. 3, no. 1, p. 10, Dec. 2010, doi: 10.1186/1754-6834-3-10.

[53] L. Johansson and J. M. Campbell, "Reproducible XPS on biopolymers: cellulose studies," *Surf. Interface Anal.*, vol. 36, no. 8, pp. 1018–1022, Aug. 2004, doi: 10.1002/sia.1827.

[54] G. Beamson and D. Briggs, *High resolution XPS of organic polymers: the Scienta ESCA300 database*. Chichester: Wiley, 1992.

[55] K. Sim, J. Lee, H. Lee, and H. J. Youn, "Flocculation behavior of cellulose nanofibrils under different salt conditions and its impact on network strength and dewatering ability," *Cellulose*, vol. 22, no. 6, pp. 3689–3700, Dec. 2015, doi: 10.1007/s10570-015-0784-y.

[56] R. Abidnejad *et al.*, "Nanocellulose-silica nanoparticles Pickering foams as leakage-free multifunctional phase change composites for energy management," *Chem. Eng. J.*, vol. 538, p. 176621, Jun. 2026, doi: 10.1016/j.cej.2026.176621.

[57] INSTITUTE OF CELLULOSE CHEMISTRY WITH WOOD RESEARCH DEPARTMENT TECHNICAL UNIVERSITY OF DARMSTADT, GERMANY, G. Jayme, G. Hunger, and INSTITUTE OF CELLULOSE CHEMISTRY WITH WOOD RESEARCH DEPARTMENT TECHNICAL UNIVERSITY OF DARMSTADT, GERMANY, "Electron Microscope 2- and 3-Dimensional Classification of Fibre Bonding," in *Trans. of the IInd Fund. Res.*

Symp. Oxford, 1961, F. Bolam, Ed., Fundamental Research Committee (FRC), Manchester, 1961, pp. 135–170. doi: 10.15376/frc.1961.1.135.

[58] A. T. Moore, L. W. Scott, I. V. deGruy, and M. L. Rollins, "The Swelling of Cotton in Water: A Microscopical Study," *Text. Res. J.*, vol. 20, no. 9, pp. 620–630, Sep. 1950, doi: 10.1177/004051755002000904.

[59] J. Cai and L. Zhang, "Rapid Dissolution of Cellulose in LiOH/Urea and NaOH/Urea Aqueous Solutions," *Macromol. Biosci.*, vol. 5, no. 6, pp. 539–548, Jun. 2005, doi: 10.1002/mabi.200400222.

[60] D. Qiang, M. Zhang, J. Li, H. Xiu, and Q. Liu, "Selective hydrolysis of cellulose for the preparation of microcrystalline cellulose by phosphotungstic acid," *Cellulose*, vol. 23, no. 2, pp. 1199–1207, Apr. 2016, doi: 10.1007/s10570-016-0858-5.

[61] J. M. B. Fernandes Diniz, M. H. Gil, and J. A. A. M. Castro, "Hornification?its origin and interpretation in wood pulps," *Wood Sci. Technol.*, vol. 37, no. 6, pp. 489–494, Apr. 2004, doi: 10.1007/s00226-003-0216-2.

[62] U. Weise, T. Maloney, and H. Paulapuro, "Quantification of water in different states of interaction with wood pulp fibres," *Cellulose*, vol. 3, no. 1, pp. 189–202, Dec. 1996, doi: 10.1007/BF02228801.

[63] C. Fu *et al.*, "Crucial role of fiber swelling in microfibrillated cellulose extraction via ball milling," *Ind. Crops Prod.*, vol. 218, p. 118899, Oct. 2024, doi: 10.1016/j.indcrop.2024.118899.

[64] F. Awaja and D. Pavel, "Recycling of PET," *Eur. Polym. J.*, vol. 41, no. 7, pp. 1453–1477, Jul. 2005, doi: 10.1016/j.eurpolymj.2005.02.005.

[65] H. Peng, Y. Sun, J. Zhang, and L. Lin, "Degradation of cellooligosaccharides in oxidative medium and alkaline medium: HPLC, FTIR, and GC-MS analyses," *BioResources*, vol. 5, no. 2, pp. 616–633, Feb. 2010, doi: 10.15376/biores.5.2.616-633.

[66] C. A. Filomeno *et al.*, "Corymbia spp. and Eucalyptus spp. essential oils have insecticidal activity against Plutella xylostella," *Ind. Crops Prod.*, vol. 109, pp. 374–383, Dec. 2017, doi: 10.1016/j.indcrop.2017.08.033.

[67] Y. Ji, Y. Peng, A. Strand, S. Fu, A. Sundberg, and E. A. Retulainen, "Fiber Evolution during Alkaline Treatment and Its Impact on Handsheet Properties," *BioResources*, vol. 13, no. 4, pp. 7310–7324, Aug. 2018, doi: 10.15376/biores.13.4.7310-7324.

[68] Y. Ji, Y. Peng, A. Strand, S. Fu, A. Sundberg, and E. A. Retulainen, "Fiber Evolution during Alkaline Treatment and Its Impact on Handsheet Properties," *BioResources*, vol. 13, no. 4, pp. 7310–7324, Aug. 2018, doi: 10.15376/biores.13.4.7310-7324.

[69] X. Wu, R. J. Moon, and A. Martini, "Crystalline cellulose elastic modulus predicted by atomistic models of uniform deformation and nanoscale indentation," *Cellulose*, vol. 20, no. 1, pp. 43–55, Feb. 2013, doi: 10.1007/s10570-012-9823-0.

[70] H. Yu, Z. Qin, B. Liang, N. Liu, Z. Zhou, and L. Chen, "Facile extraction of thermally stable cellulose nanocrystals with a high yield of 93% through hydrochloric acid hydrolysis under hydrothermal conditions," *J. Mater. Chem. A*, vol. 1, no. 12, p. 3938, 2013, doi: 10.1039/c3ta01150j.

[71] R. Mitchell, C. M. Carr, M. Parfitt, J. C. Vickerman, and C. Jones, "Surface chemical analysis of raw cotton fibres and associated

materials," *Cellulose*, vol. 12, no. 6, pp. 629–639, Dec. 2005, doi: 10.1007/s10570-005-9000-9.

[72] L. Fras, L.-S. Johansson, P. Stenius, J. Laine, K. Stana-Kleinschek, and V. Ribitsch, "Analysis of the oxidation of cellulose fibres by titration and XPS," *Colloids Surf. Physicochem. Eng. Asp.*, vol. 260, no. 1–3, pp. 101–108, Jun. 2005, doi: 10.1016/j.colsurfa.2005.01.035.

[73] M. Pääkkö *et al.*, "Enzymatic Hydrolysis Combined with Mechanical Shearing and High-Pressure Homogenization for Nanoscale Cellulose Fibrils and Strong Gels," *Biomacromolecules*, vol. 8, no. 6, pp. 1934–1941, Jun. 2007, doi: 10.1021/bm061215p.

[74] M. Schenker, J. Schoelkopf, P. Gane, and P. Mangin, "Rheology of microfibrillated cellulose (MFC) suspensions: influence of the degree of fibrillation and residual fibre content on flow and viscoelastic properties," *Cellulose*, vol. 26, no. 2, pp. 845–860, Jan. 2019, doi: 10.1007/s10570-018-2117-4.

[75] A. S. Ospennikov, A. L. Kwiatkowski, and O. E. Philippova, "Cellulose Nanofibrils vs Nanocrystals: Rheology of Suspensions and Hydrogels," *Gels*, vol. 11, no. 11, p. 926, Nov. 2025, doi: 10.3390/gels11110926.

[76] M. Çiçekler and A. Tutuş, "Hornification in Recycled Fibers and Its Impacts on Quality and Recycling Efficiency," Feb. 2025, doi: 10.5281/ZENODO.14930709.

[77] R. G. Larson, *The structure and rheology of complex fluids*. in Topics in chemical engineering. New York: Oxford University Press, 1999.

[78] A. I. Koponen, "The effect of consistency on the shear rheology of micro- and nanofibrillated cellulose suspensions: A review".

[79] W. P. Cox and E. H. Merz, "Correlation of dynamic and steady flow viscosities," *J. Polym. Sci.*, vol. 28, no. 118, pp. 619–622, Apr. 1958, doi: 10.1002/pol.1958.1202811812.

Appendices

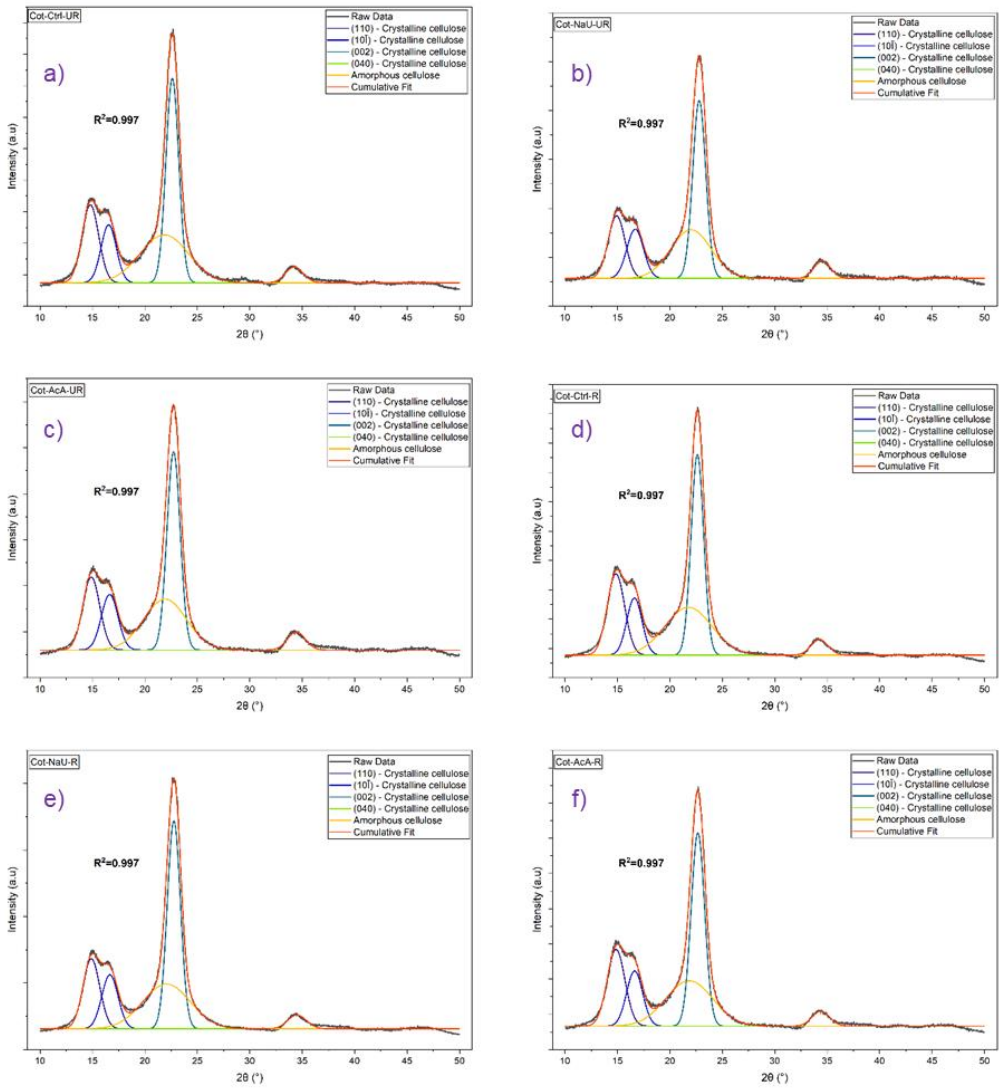

Appendix A: Gaussian peak deconvolution of XRD diffractograms for cotton samples (a) Cot-Ctrl-UR, (b) Cot-NaU-UR, (c) Cot-AcA-UR, (d) Cot-Ctrl-R, (e) Cot-NaU-R, and (f) Cot-AcA-R. Coloured curves: individual crystalline Gaussians (1$\bar{1}$0), (110), (002), (040); grey filled peak: amorphous component; black line: summed fit. All fits $R^2 \geq 0.995$.

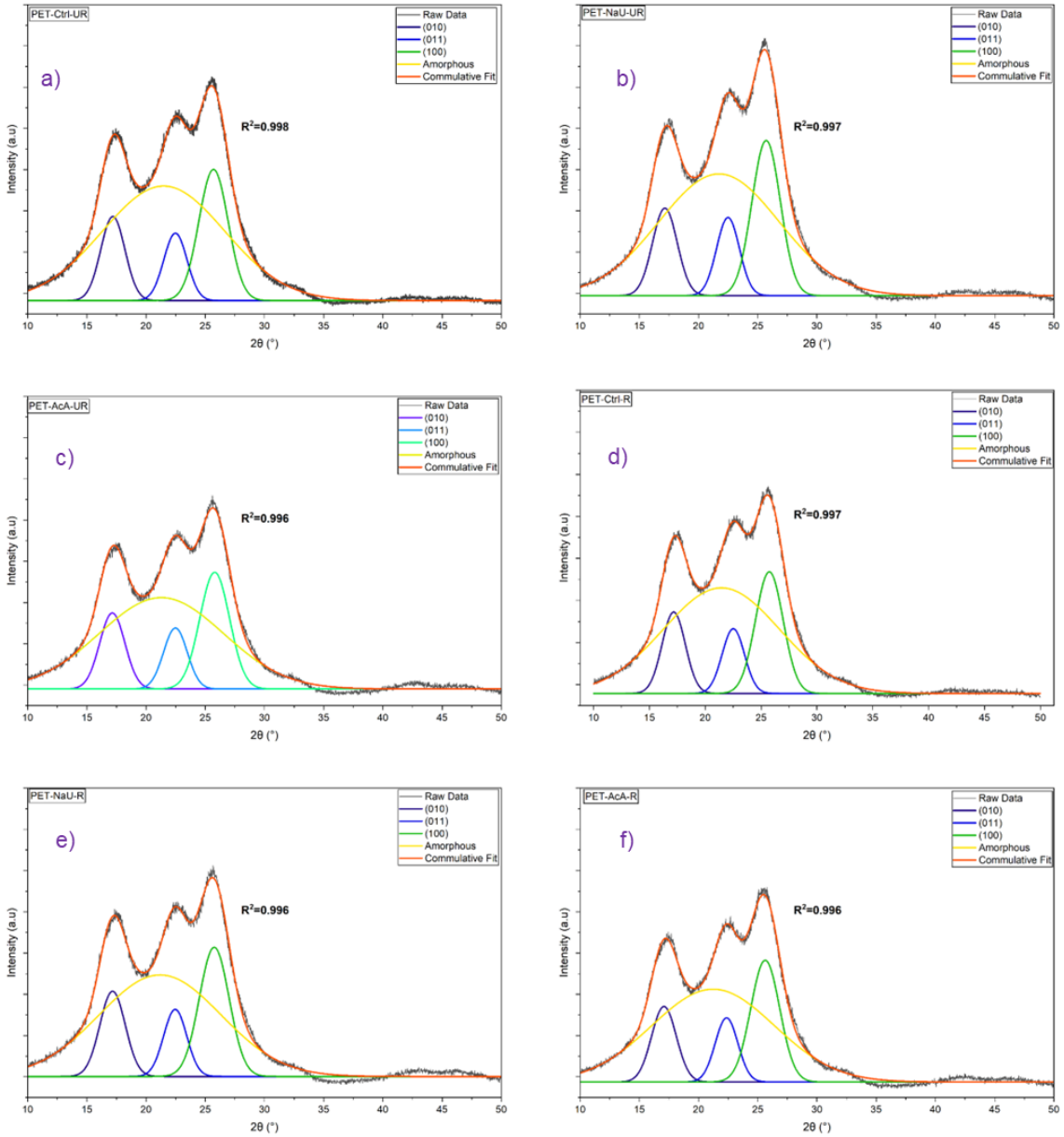

Appendix B: Gaussian peak deconvolution of XRD diffractograms for PET samples (a) PET-Ctrl-UR, (b) PET-NaU-UR, (c) PET-AcA-UR, (d) PET-Ctrl-R, (e) PET-NaU-R, and (f) PET-AcA-R. Coloured curves: triclinic PET crystalline reflections ($1\bar{1}0$)/(010), (110), (100); grey filled peak: amorphous component; black line: summed fit.

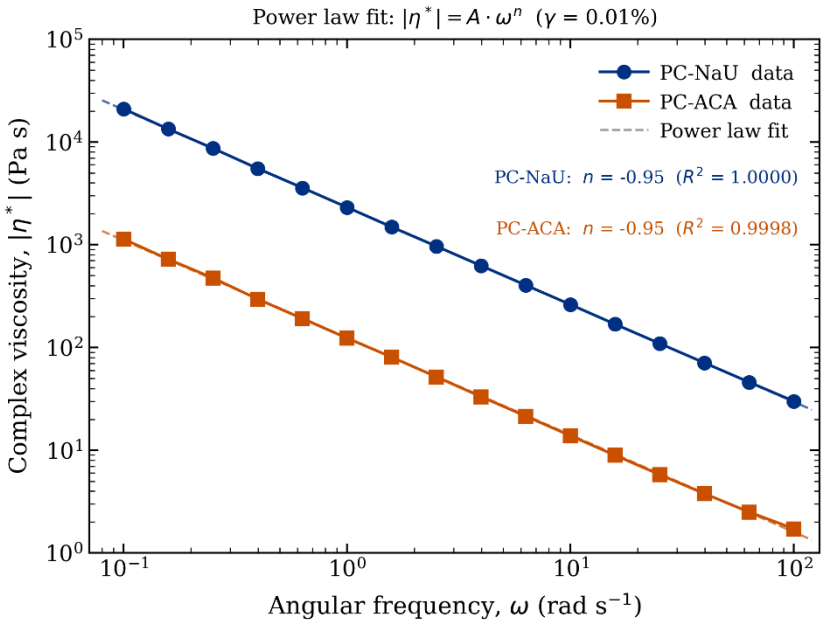

Appendix C: Complex viscosity (|η*|) vs angular frequency (ω) for PC-NaU and PC-ACA at γ = 0.01%. Solid lines: power law fits (Eq. 6); fit parameters: PC-NaU — A = 2,321 Pa·s, n = −0.95; PC-ACA — A = 125 Pa·s, n = −0.95 (both R^2 > 0.999).

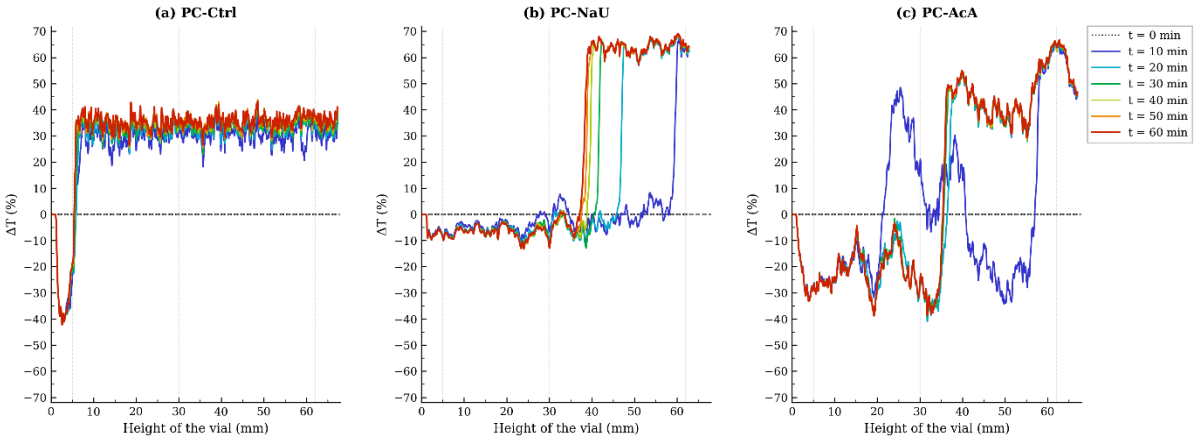

Appendix D: ΔT vs height profiles at t = 0, 10, 20, 30, 40, 50, and 60 min for (a) PC-Control, (b) PC-NaOH/Urea, and (c) PC-Acetic Acid at 0.2 wt% concentration. *Positive ΔT = local clarification; negative ΔT = local accumulation. Dashed vertical line: ΔT = 0.*

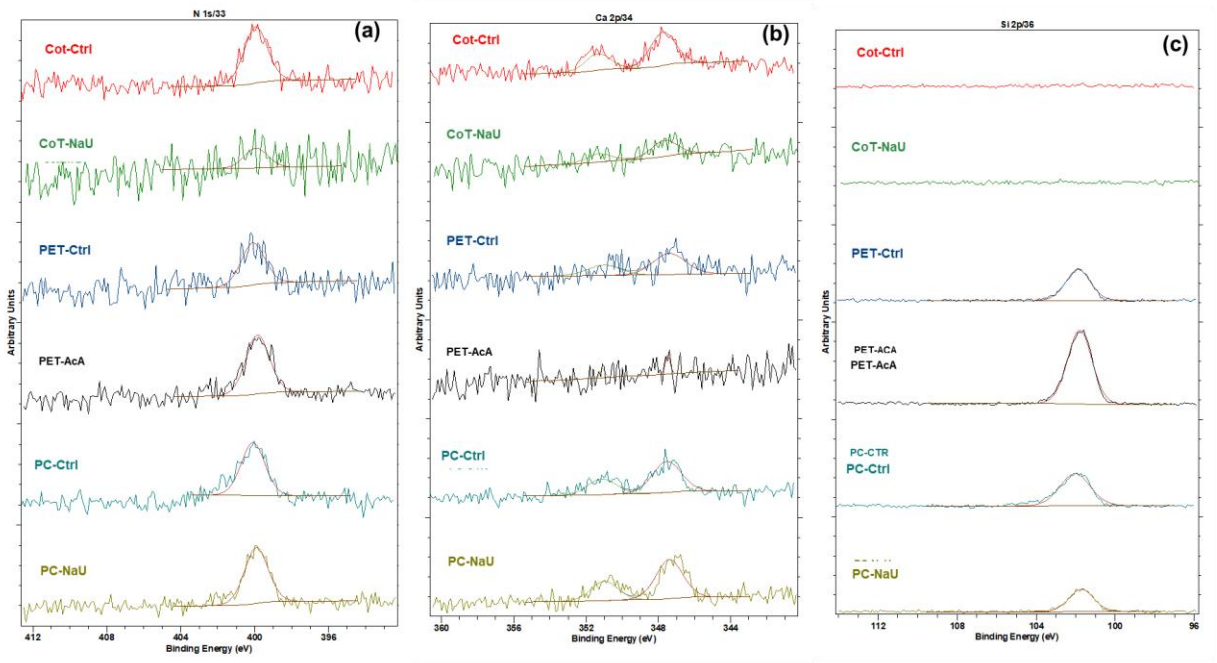

Appendix E: High-resolution XPS spectra of trace elements for all six samples: (a) N 1s — peak at ~399.9 eV assigned to amine-type nitrogen, near-completely eliminated in COT-NaU confirming alkaline removal of nitrogenous surface contaminants; (b) Ca 2p — doublet at ~347.7 eV assigned to ionic Ca^{2+}, reduced in COT-NaU consistent with removal of calcium pectates; (c) Si 2p — signal at ~101.9 eV characteristic of a silicone-type surface finish, detected exclusively on PET-containing samples and absent on cotton, confirming a PET-associated finish unaffected by either pretreatment.